Part I: Bayesian inversion algorithm for estimating local variations in permeability and porosity of reinforcements using experimental data

M.Y. Matveev[a], A. Endruweit[a], A.C. Long[a], M.A. Iglesias[b], M.V. Tretyakov[b]

[a] *Composites Group, Faculty of Engineering, University of Nottingham, Nottingham, UK*
[b] *School of Mathematical Sciences, University of Nottingham, Nottingham, UK*

Abstract

A novel regularising ensemble Kalman filter algorithm based on the Bayesian paradigm is applied to RTM processes to estimate local permeability and porosity of fibrous reinforcements using data (pressure and flow front positions) collected during resin injection. The algorithm allows to detect locations of defects in the preform. It is tested in two virtual experiments, one with the simple geometry of a two-dimensional rectangular preform and the other with a more complex 3D geometry. The first geometry also plays the role of a digital twin for the lab experiment used for further testing. In both the virtual and lab experiments, it is demonstrated that the considered methodology is able to successfully discover defects and estimate local permeability and porosity and, hence can be used to improve nondestructive examination of composites.

Keywords: Resin transfer moulding, random permeability and porosity, nondestructive examination of composites, ensemble Kalman filter, uncertainty quantification.

1. Introduction

Resin transfer moulding (RTM) processes give a cost-effective and versatile way for manufacturing components from composite materials. However, it is well known (see e.g. [1–6] and references therein) that composites may have substantial variability of material properties and appearance of defects which is not acceptable, especially for high-value components. Nondestructive examination (NDE) is vital for ensuring that manufactured composite parts satisfy requirements imposed on their mechanical properties. Currently, NDE is performed using measurements (e.g. X-ray or ultrasonic C-Scan) after RTM, and it can take up to 10% to 30% [7] of the total production time for composite parts.

Here, it is suggested to use in-process information (pressure values and resin arrival at several positions and time moments) collected during resin injection and a novel property inversion algorithm to estimate local permeability and porosity. Based on these estimations, locations of defects in the preform are identified which can be used for improving and accelerating NDE.

The inversion algorithm is constructed using a novel regularising ensemble Kalman filter algorithm (REnKA) [8] and ideas of Bayesian level set methods for geometric inverse problems [9, 10]. The algorithm is based on the recently developed infinite-dimensional Bayesian theory [11] which allows to treat inverse problems arising in complex problems, like estimation of unknown permeability and porosity of a preform in RTM process.

This part of the report is organised as follows. In Section 2, we describe the methodology based on the Bayesian paradigm which we apply in Sections 3 and 4 to estimate permeability and porosity using data observed during RTM process. In Section 3, we consider virtual experiments where data are obtained

Email addresses: Mikhail.Matveev@nottingham.ac.uk (M.Y. Matveev), Andreas.Endruweit@nottingham.ac.uk (A. Endruweit), Andrew.Long@nottingham.ac.uk (A.C. Long), Marco.Iglesias@nottingham.ac.uk (M.A. Iglesias), Michael.Tretyakov@nottingham.ac.uk (M.V. Tretyakov)

from simulating RTM processes using Ansys Fluent©. We consider two geometries: a flat rectangular preform and a 3D geometry. The former plays the role of a digital twin for lab experiments which are considered in Section 4. Conclusions and discussions are in the last section. Appendices contain additional mathematical details supporting the description of the Bayesian inversion algorithm from Section 2.

2. Bayesian inversion algorithm

In this section, we introduce the methodology to infer the (possibly heterogeneous) porosity $\varphi(x)$ and permeability $K(x)$ of a fibre preform from measurements of resin pressure and moving front location collected during the infusion process. The methodology is based on the recently developed infinite-dimensional Bayesian theory [11] and algorithms [8, 9, 12] for data assimilation required for complex models describing spatial physical phenomena. To provide an intuition-based explanation behind the algorithm used here, we start with subsection 2.1 where we discuss Bayesian inversion idea on the physical level of rigour. We present its formal mathematical formulation in Subsections 2.2-2.4.

2.1. Introductory description of the algorithm

The idea of Bayesian inversion algorithms within the context of RTM is as follows. Assume that measurements of pressure at some locations in the preform and/or of front positions at some time moments are available during the RTM process. A Bayesian inversion algorithm starts with a prior distribution (in the Bayesian Statistics language: an initial guess) of local permeability and porosity. This distribution is characterised by a set of samples (in other words, ensemble of particles) of these material properties weighted with their probabilities. Then, based on the results of numerical RTM simulations of the samples and measurements, the Bayesian inversion algorithm iteratively evolves these samples (updating the distribution of local permeability and porosity) so that the samples become consistent with the measurements (see Fig. 1). Using the obtained updated samples of the predicted distribution (in the Bayesian statistics language: posterior distribution), we compute estimates for local permeability and porosity together with their variances, which, in turn, provide a measure of uncertainty (error) of the found estimates.

To summarise, the inputs for the algorithm are measurements obtained during the RTM process, the geometry of the preform, a numerical RTM model and the prior distribution for local permeability and porosity. These are based on available prior knowledge of permeability and porosity (e.g., their values according to the design and expected level of variability) but otherwise they are random/unknown. The output of the algorithm is a posterior distribution of local permeability and porosity, i.e. their probability distribution conditioned on available observations, which can be used for finding expected local permeability and porosity together with their confidence intervals and thus identify location of defects in the preform.

In contrast to deterministic approaches (see e.g. [13, 14] and references therein) where only single estimates are obtained (e.g. most likely local permeability and porosity), the Bayesian framework approximates the distribution of local permeability and porosity conditioned on the measurements. In other words, it provides an entire set of possible local permeabilities and porosities together with their probabilities of occurrence. Probabilistic knowledge of material properties enables uncertainty quantification which is crucial for decision making within the manufacturing process. Based on the outcomes from the Bayesian methodology, one can compute, for instance, the probability of having defects of certain size defined by a tolerance.

In comparison with Machine Learning approaches, the Bayesian inversion paradigm used here does not require training as it uses the physical model of the process (where the physical model can be understood as e.g., PAM-COMPOSITES© or Ansys Fluent© solvers for resin injection). Since it does not rely on training, it can cope with new scenarios, not observed before in experiments or simulations.

In the next three subsections we mathematically formalise application of Bayesian inversion methodology to RTM.

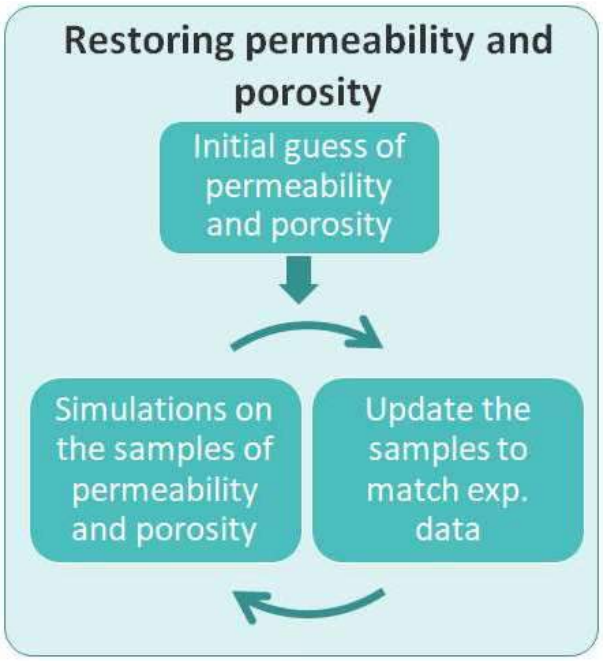

Figure 1: Schematic illustration of Bayesian inversion algorithms.

2.2. Parameterisation to infer defects

The selection of the prior (initial guess) in the Bayesian algorithm described above is crucial for accurate estimation of physical properties (of the material). Choosing priors is particularly challenging in cases where these properties display complex geometric features and/or abrupt discontinuities that arise from, for example, the presence of material defects. To address this challenge, we apply a level-set technique that enables to parameterise local properties with sharp discontinuities and, when combined within the modern Bayesian methodology [9], allows to infer the geometry of regions with different material properties. Our aim is to use such a technique to identify material defects which are often associated with higher (including race-tracking) or lower permeability and porosity.

In Figure 2 we illustrate the idea behind the level-set parameterisation in a 2D domain. An underlying level-set function (Figure 2, left) is introduced to parameterise, via truncation at the zero level, the piecewise constant porosity of Figure 2 (middle). The region with high porosity (Region 1) corresponds to positive values of the level-set function while lower porosity values (Region 2) corresponds to negative values of the zero level-set. Heterogeneity within each region can also be incorporated by simply assigning heterogenous functions with different mean values in each of those regions (see Figure 2 (right)). The inference problem that we wish to solve is to find (i) the underlying level-set function $\xi(x)$ that defines the geometry of defects; (ii) functions $\varphi_1(x)$ and $\kappa_1(x)$ that characterise porosity and permeability within the defects, respectively; and (iii) functions $\varphi_2(x)$ and $\kappa_2(x)$ for porosity and permeability in the background field. The set of unknowns for the inference/inverse problem is expressed in the following (function) variable

$$u(x) = (\varphi_1(x), \varphi_2(x), \kappa_1(x), \kappa_2(x), \xi(x)). \tag{2.1}$$

We propose parameterisations of $\varphi(x)$ and $K(x)$ which enable to statistically identify material defects associated with discontinuities and abrupt changes in these physical properties of the preform. The inference problem is posed in terms of the Bayesian calibration of a parameter-to-output map, $\mathcal{G}$, that takes those parameters which define porosity and permeability $(\varphi(x), K(x))$ and maps them into a variable, d,

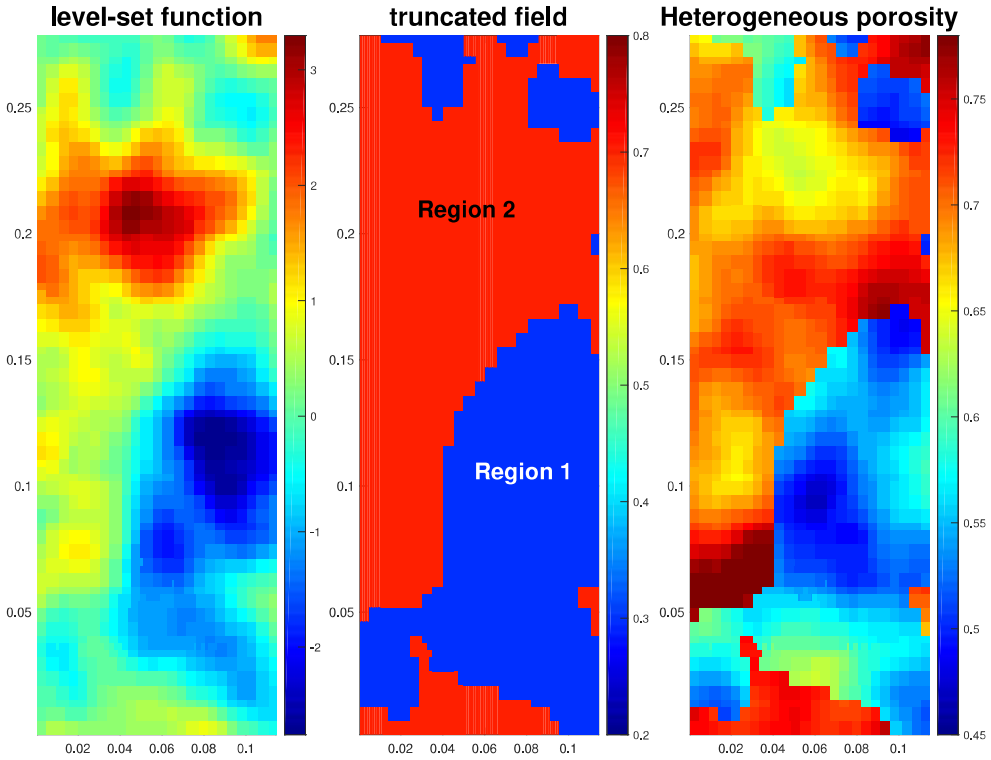

Figure 2: Level-set parametrisation of defects in a 2D preform: level-set function (left); truncated level-set function defining regions of porosity (middle); heterogeneous field with two regions (right).

that comprises predictions of pressure and front from sensors monitored at a set of specific times during the resin infusion (see Appendix A).

In Appendix A, we define a map $\mathcal{F}$ that arises from the simulation of the aforementioned predictions of pressure and flow front for given porosity and permeability fields. With the aid of this map, the direct (or in other words, forward) problem can be stated as follows: for given porosity $\varphi(x)$ and permeability $K(x)$ of the preform, compute/simulate d defined by

$$d = \mathcal{F}(\varphi, K), \tag{2.2}$$

where we have dropped the dependence of φ and K on the independent variable x, in order to emphasise that the parameter-to-output map $\mathcal{F}$ is a relation defined for functions rather than only for the values of these functions. Within the RTM setting (see Appendix A), d consists of pressure and flow front position.

Our aim is to solve the following inverse problem: for given measurements, possibly corrupted by noise, of d defined in (2.2), find $K(x)$ and $\varphi(x)$. We assume that these measurements, denoted by d^η, satisfy

$$d^\eta = \mathcal{F}(\varphi, K) + \eta, \tag{2.3}$$

where η is a vector of random noise. We use the standard assumption that η follows a Gaussian distribution with zero mean and covariance Γ (we denote this by $\eta \sim N(0, \Gamma)$). Note that equation (2.3) simply states that, in the absence of modelling errors, the empirical measurements d^η, can be obtained from the predictions of the RTM model by accounting for an additive random error in those predictions.

We introduce a parameterisation of $K(x)$ and $\varphi(x)$ that will enable us to identify, via the solution of the inverse problem, the location and properties of material defects. To this end, consider a level-set

parameterisation [9] of $K(x)$ in terms of three unknown functions $\kappa_1(x)$, $\kappa_2(x)$ and $\xi(x)$ as follows

$$K(x) = \kappa_1(x) + (\kappa_2(x) - \kappa_1(x))\mathbb{1}_{A_\xi}(x), \tag{2.4}$$

where $\mathbb{1}_{A_\xi}(x)$ is the indicator function of the set $A_\xi = \{x \in \mathbb{R}^3 | \xi(x) > 0\}$, i.e.

$$\mathbb{1}_{A_\xi}(x) = \begin{cases} 1 & \text{if } x \in A_\xi, \\ 0 & \text{if } x \notin A_\xi. \end{cases}$$

Similarly, we parameterise the porosity $\varphi(x)$ in terms of functions $\varphi_1(x)$, $\varphi_2(x)$ and $\xi(x)$, via the following expression:

$$\varphi(x) = \varphi_1(x) + (\varphi_2(x) - \varphi_1(x))\mathbb{1}_{A_\xi}(x). \tag{2.5}$$

In expressions (2.4)-(2.5), $\xi(x)$ is the so-called level set function that allows us to parameterise the domain of any material that has two regions, R_1 and R_2, with substantially different (heterogenous) permeability and porosity, (φ_1, κ_1) and (φ_2, κ_2), respectively. The aim of such a parameterisation is to infer possible regions of low or high permeability that arise from the presence of material defects. It is important to mention that the parameterisations (2.4)-(2.5) also incorporate variability of permeability and porosity within each of those regions.

We now reformulate the inverse problem defined earlier (for K and φ) in terms of the unknown functions which parameterise K and ϕ, and which we express in the following (function) variable:

$$u = (\varphi_1, \varphi_2, \kappa_1, \kappa_2, \xi). \tag{2.6}$$

By noticing that the parameterisations (2.4)-(2.5) induces a map Θ:

$$u \to \Theta(u) = (\varphi, K),$$

we can thus rewrite (2.3) in terms of the parameter-to-output map $\mathcal{G} = \mathcal{F} \circ \Theta$ as follows

$$d^\eta = \mathcal{F}(\varphi, \kappa) + \eta = \mathcal{F}(\Theta(u)) + \eta = \mathcal{G}(u) + \eta. \tag{2.7}$$

Finally, we use expression (2.7) to formulate the inverse problem of finding u for given measurements d^η. Once $u = (\varphi_1, \varphi_2, \kappa_1, \kappa_2, \xi)$ has been found, expressions (2.4)-(2.5) can be used to find K, ϕ and, more importantly, identify the local variability of these properties corresponding to possible material defects. In the subsequent section we address this inverse problem in a Bayesian setting.

2.3. The Bayesian approach

The solution to the inverse problem stated earlier is not unique; a whole set of functions $u = (\varphi_1, \varphi_2, \kappa_1, \kappa_2, \xi)$ may be consistent with the observed data d^η in the sense of (2.7). Therefore, a deterministic approach that produces one single estimate of u is not desirable, since it can overlook a possible range of admissible solutions. We consider a probabilistic framework that allows us to compute a distribution of those functions and thus facilitates the quantification of uncertainties associated with our estimates. More specifically, we adopt the Bayesian framework [11] in which $u(x)$ is a random function with a specified prior probability distribution $\mathbb{P}(u)$. The prior encompasses our probabilistic knowledge of the material properties of the preform, prior to the collection of data (i.e., before the resin injection). For example, the prior may incorporate design values of permeability and porosity as well as regions where defects are more likely to be present. We refer the reader to Appendix B, where we construct this distribution and discuss algorithms to produce the corresponding samples.

In the Bayesian framework, the solution to an inverse problem is the conditional (posterior) distribution of the unknown $u(x)$ for given d^η. The posterior, denoted by $\mathbb{P}(u|d^\eta)$, can be expressed via Bayes' rule as follows [11]:

$$\mathbb{P}(u|d^\eta) = \frac{\mathbb{P}(d^\eta|u)\mathbb{P}(u)}{\mathbb{P}(d^\eta)}, \tag{2.8}$$

where $\mathbb{P}(d^\eta|u)$ is the likelihood, namely, the probability of the observed measurements d^η given a particular realisation of the unknown $u(x)$. The term $\mathbb{P}(d^\eta)$ in (2.4) denotes the probability of d^η; this term is a normalisation constant defined by

$$\mathbb{P}(d^\eta) = \int \mathbb{P}(d^\eta|u)\mathbb{P}(du). \tag{2.9}$$

From (2.7) and our assumption on the distribution of η, it follows that $d^\eta|u \sim N(\mathcal{G}(u), \Gamma)$ and thus (2.8) becomes

$$\mathbb{P}(u|d^\eta) = \frac{1}{Z}\mathbb{P}(u)\exp\big[-\frac{1}{2}||\Gamma^{-1/2}(d^\eta - \mathcal{G}(u))||^2\big], \tag{2.10}$$

where

$$Z = \int \mathbb{P}(u)\exp\big[-\frac{1}{2}||\Gamma^{-1/2}(d^\eta - \mathcal{G}(u))||^2\big]du. \tag{2.11}$$

Given a prior, expression (2.10) provides the posterior $\mathbb{P}(u|d^\eta)$ up to the normalisation constant (2.11). Due to the nonlinearity of the parameter-to-output map $\mathcal{G}$ which appears in (2.11), this normalisation constant, in general, cannot be computed analytically, and so the resulting posterior distribution $\mathbb{P}(u|d^\eta)$ cannot be expressed in a closed form. Sampling methods then need to be applied for the approximation of the Bayesian posterior [12]. In the next section a regularising ensemble Kalman algorithm of [8] is introduced to provide a sampling approximation of the posterior.

For the sake of clarity in the previous exposition, we have considered an all-at-once version of the Bayesian framework for which all the observations collected during the resin infusion are used to infer porosity and permeability. However, the framework can be used in a sequential fashion to enable the online estimation of these properties [8, 12].

2.4. The regularising ensemble Kalman algorithm

In order to compute a numerical approximation of the Bayesian posterior defined in (2.10) we use the regularising ensemble Kalman algorithm (REnKA) recently proposed in [8]. The work [8] has shown that REnKA provides, at a reasonable computational cost, accurate approximations of the Bayesian posterior that arises from RTM processes. This algorithm was derived via Gaussian approximations within the adaptive tempering Sequential Monte Carlo (SMC) scheme [12]. Although numerous sampling methods exist for approximating the Bayesian posterior, the SMC framework of [12] is tailored to address high-dimensional Bayesian inverse problems such as the one described in the previous subsection. Indeed, we note that the approximation of (2.10) requires the discretisation of $u(x)$ at every point of the computational domain (which in turn involves the discretisation of φ_1, φ_2, κ_1, κ_2 and ξ). Therefore, the posterior is defined on a high dimensional space (e.g. 10^5).

The adaptive tempering SMC framework of [12] consists of approximating a sequence of intermediate distributions between prior and posterior defined by

$$\mu_n(u) = \frac{1}{Z}\mathbb{P}(u)\exp\Big[-\frac{\phi_n}{2}||\Gamma^{-1/2}(d^\eta - \mathcal{G}(u))||^2\Big], \tag{2.12}$$

where $\{\phi_n\}_{n=0}^q$ is a sequence of $q+1$ tempering parameters that satisfy $0 = \phi_0 < \phi_1 < \cdots < \phi_q = 1$. Note that $n = 0$ and $n = q$ in (2.12) yield the prior ($\mu_0 = \mathbb{P}(u)$) and posterior ($\mu_q = \mathbb{P}(u|d^\eta)$ (see (2.10)), respectively. From definition (2.12), it follows that

$$\frac{\mu_{n+1}(u)}{\mu_n(u)} = \exp\Big[-\frac{(\phi_{n+1} - \phi_n)}{2}||\Gamma^{-1/2}(d^\eta - \mathcal{G}(u))||^2\Big] \tag{2.13}$$

$$= \exp\Big[-\frac{1}{2}||(\alpha_n\Gamma)^{-1/2}(d^\eta - \mathcal{G}(u))||^2\Big], \tag{2.14}$$

where

$$\alpha_n = \frac{1}{(\phi_{n+1} - \phi_n)}. \tag{2.15}$$

Starting with an initial ensemble, $\{u_0^{(j)}\}_{j=1}^J$, of J samples from the prior $\mu_0(u) = \mathbb{P}(u)$, REnKA uses a sample-based Gaussian approximation of each $\mu_n(u)$ defined in (2.12) to update, via a linearisation of the recursive formula in (2.13), the ensemble of particles that approximate distribution $\mu_{n+1}(u)$. Upon convergence, REnKA produces an ensemble $\{u^{(j)}\}_{j=1}^J$ that provides an approximation to the posterior (2.10) which can, in turn, be used to compute statistical quantities of the porosity and permeability (see details below). The parameter α_n in (2.15) controls the number of intermediate distributions μ_n needed for stability and accuracy of the algorithm. We refer the reader to [8] for further details on selection strategies for this parameter.

REnKA is displayed in Algorithm 1. We note that it can be used in a black-box fashion. The total cost of REnKA is given by $c = J \times q$ RTM simulations, where, as before, q is the total number of iterations (i.e. the number of intermediate distributions μ_n). Our experiments suggest that an ensemble of size $J \approx 100$ is sufficient to provide accurate approximations of the posterior usually within $q = 10$ iterations. Therefore, the total cost is approximately 10^3 number of simulation runs. We note that REnKA scales with respect to the number of particles J, and so its computational execution time can be substantially reduced via the use of high-performance or parallel computing.

The ensemble of particles obtained via REnKA (Algorithm 1) can be used to compute an approximation to the posterior expectations of u. For example, given the final ensemble (upon convergence) $\{u^{(j)}\}_{j=1}^J = \{(\varphi_1^{(j)}, \varphi_2^{(j)}, \kappa_1^{(j)}, \kappa_2^{(j)}, \xi^{(j)})\}_{j=1}^J$, we can compute the posterior mean $\overline{u}(x)$ defined by

$$\overline{u}(x) = (\overline{\varphi}_1(x), \overline{\varphi}_2(x), \overline{\kappa}_1(x), \overline{\kappa}_2(x), \overline{\xi}(x)) = \frac{1}{J}\sum_{j=1}^{J}(\varphi_1^{(j)}(x), \varphi_2^{(j)}(x), \kappa_1^{(j)}(x), \kappa_2^{(j)}(x), \xi^{(j)}(x)). \tag{2.16}$$

A posterior estimator of porosity and permeability can be computed via expressions (2.4)-(2.5) applied to $\overline{u}$, i.e.

$$\varphi^*(x) = \overline{\varphi}_1(x) + (\overline{\varphi}_2(x) - \overline{\varphi}_1(x))\mathbb{1}_{A_{\overline{\xi}}}(x), \tag{2.17}$$

$$K^*(x) = \overline{\kappa}_1(x) + (\overline{\kappa}_2(x) - \overline{\kappa}_1(x))\mathbb{1}_{A_{\overline{\xi}}}(x). \tag{2.18}$$

We can additionally compute the posterior distributions of K and φ from the ensemble of $\{u^{(j)}\}_{j=1}^J$. More specifically, we use (2.4) to compute the posterior ensemble of permeability

$$K^{(j)}(x) = \kappa_1^{(j)}(x) + (\kappa_2^{(j)}(x) - \kappa_1^{(j)}(x))\mathbb{1}_{A_{\xi^{(j)}}}(x), \qquad j = 1, \ldots, J. \tag{2.19}$$

The posterior (ensemble) mean and variance of permeability can be computed via

$$\overline{K}(x) = \frac{1}{J}\sum_{j=1}^{J} K^{(j)}(x), \qquad \sigma_K^2(x) = \frac{1}{J}\sum_{j=1}^{J}(K^{(j)}(x) - \overline{K}(x))^2. \tag{2.20}$$

From (2.5), we can compute the ensemble of posterior porosity $\{\varphi^{(j)(x)}\}_{j=1}^J$ and, with analogous formulas to those in (2.20), we can compute the corresponding posterior mean and variance $\overline{\varphi}(x)$ and $\sigma_\phi^2(x)$, respectively. We emphasise, by means of the dependence on x in (2.20), that statistical measures of the unknown properties are, in general, functions of the spatial domain of the preform. Incorporating variability in those properties is crucial to identify locations of material defects.

Finally, we use the posterior ensemble of porosity and permeability $\{K^{(j)}(x)\}_{j=1}^J$ and $\{\varphi^{(j)(x)}\}_{j=1}^J$ to approximate the posterior distribution of measurement predictions. This is conducted via the map $\mathcal{F}$ discussed earlier which, in turn, involves the simulation of an ensemble of model predictions

$$d^{(j)} = \mathcal{F}(K^{(j)}, \varphi^{(j)}), \qquad j = 1, \ldots, J. \tag{2.21}$$

The distribution of measurement model predictions characterised by the ensemble $\{d^{(j)}\}_{j=1}^J$ is used to assess whether the posterior distribution of material properties results in predictions which are consistent with the data.

Algorithm 1 Regularising ensemble Kalman Algorithm

Let $\{u_0^{(j)}\}_{j=1}^J$ be the initial ensemble of J elements. Let $d^\eta \in \mathbb{R}^M$ the vector of M measurements. Let Γ be the measurements' error covariance.

Set $t_0 = 0$
while $t_n < 1$ **do**
(1) **Prediction step.** Evaluate

$$\mathcal{G}_n^{(j)} = \mathcal{G}(u_n^{(j)}), \qquad j \in \{1, \dots, N_e\} \tag{2.22}$$

and define $\overline{\mathcal{G}}_n = \frac{1}{J}\sum_{j=1}^J \mathcal{G}_n^{(j)}$
(2) **Compute regularisation parameter** α_n**:**.

$$\alpha_n^* = \frac{1}{M}\frac{1}{J}\sum_{j=1}^J ||\Gamma^{-1/2}(d^\eta - \mathcal{G}_n^{(j)})||^2$$

if $t_n + \frac{1}{\alpha_n^*} \geq 1$ **then** Set $\alpha_n = \frac{1}{1-t_n}$, $t_{n+1} = 1$.
else Set $\alpha_n = \alpha_n^*$, $t_{n+1} = t_n + \frac{1}{\alpha_n}$.
end if
(3)**Analysis step.** Define $C_n^{u\mathcal{G}}$, $C_n^{\mathcal{G}\mathcal{G}}$ by

$$C_n^{\mathcal{G}\mathcal{G}}(\cdot) = \frac{1}{J-1}\sum_{j=1}^J (\mathcal{G}(u_n^{(j)}) - \overline{\mathcal{G}}_n)(\mathcal{G}(u_n^{(j)}) - \overline{w}_n)^T \tag{2.23}$$

$$C_n^{u\mathcal{G}}(\cdot) = \frac{1}{J-1}\sum_{j=1}^J (u_n^{(j)} - \overline{u}_n)(\mathcal{G}(u_n^{(j)}) - \overline{\mathcal{G}}_n)^T. \tag{2.24}$$

Update each ensemble member:

$$u_{n+1}^{(j)} = u_n^{(j)} + C_n^{u\mathcal{G}}(C_n^{\mathcal{G}\mathcal{G}} + \alpha_n\Gamma)^{-1}(y^\eta - \mathcal{G}_n^{(j)} + \eta_n^{(j)}), \qquad j \in \{1, \dots, J\} \tag{2.25}$$

where $\eta_n^{(j)} \sim N(0, \Gamma)$.
$n + 1 \to n$
end while

3. Validation in virtual experiments

In this section, we test Algorithm 1 in virtual experiments, i.e., using computer generated data. To this end, the ANSYS Fluent© solver is used to model a real RTM process. A number of pressure and resin arrival virtual sensors are programmed using a user-defined-function (UDF) written in C for ANSYS Fluent©. During the run of the ANSYS Fluent© solver, data from the sensors are collected, which are then used as input for the inversion algorithm. The purpose of the virtual experiments is to confirm whether REnKA can detect locations of defects and give reasonable estimates for local permeability and porosity. Two examples of preforms are considered. The first example (subsection 3.1) is a flat rectangular preform. Its geometry is identical to the one used in the lab experiments (Section 4) and hence it plays the role of a digital twin here. The second example (subsection 3.2) has a more complex 3D geometry of an abstracted transmission tunnel; it is more realistic from the practical point of view and more challenging for Bayesian inversion algorithms.

3.1. Rectangular part

Flow through a rectangular porous preform inside an RTM tool was simulated using a transient two-phase flow model within ANSYS Fluent©. It was assumed that the permeability of the reinforcement does not change with time (no compaction or decompaction, no change of properties with saturation) but can change from point to point. Viscosity of the fluid remained constant (i.e., the process is assumed to be isothermal with no resin cure present) and was set to 0.1 Pa·s. No-slip boundary conditions were imposed at the walls of the cavity. A constant pressure of 0.4 bar is set at the inlets and 0 bar at the outlet. Finally, the model was assumed to neglect any through-thickness effects which made it possible to use a 2D implementation of the numerical algorithm. The permeability is assumed to stay constant within each element of the mesh used in simulations but can vary between the elements, which was implemented via a UDF extension. A schematic drawing of a rectangular mould is shown in Fig. 3 (left). Six pressure sensors and seven equally spaced linear flow sensors are placed within the tool.

Mesh convergence studies were performed, and the mesh sufficient to obtain accurate results is shown in Fig. 3 (right). The ANSYS Fluent© solver settings were: pressure-based solver; implicit VOF formulation; SIMPLE algorithm for pressure-velocity coupling; spatial discretisation of gradient using Green-Gauss Node Based gradient method; spatial discretisation of pressure and momentum using PRESTO! and third-order MUSCL methods, discretisation of volume fraction using modified HRIC method. Under-relaxation and convergence settings were kept to their default values.

The aim of this experiment is to identify material defects of a rectangular part. We assume that the reinforcement contains two circular defects of radius $r = 0.025$ m and centres with coordinates $(0.017\text{ m}, 0.083\text{ m})$ and $(0.03\text{ m}, 0.18\text{ m})$, respectively. We construct the true porosity $\varphi^\dagger(x)$ and permeability $K^\dagger(x)$ (i.e. the ones we wish to infer) so that these properties have lower permeability and porosity in the defects than those in the background (region without defects). In order to account for real-case scenarios where porosity and permeability may display variability (within the defects and the background regions), we assume the porosity and permeability in both defects and background are Gaussian random fields (see Appendix B). The plots of $\varphi^\dagger(x)$ and $K^\dagger(x)$ are displayed in the left and left-middle panels of Fig. 4.

We use $\varphi^\dagger(x)$ and $K^\dagger(x)$ to generate virtual data (measurements of pressure and flow front position) which we subsequently use via REnKA to infer those material properties. To this end, we run the RTM simulator (see Appendix A) with permeability and porosity specified by $K^\dagger$ and $\varphi^\dagger$ to produce noise-free predictions of pressure and front location d. These predictions are then superimposed with a vector Gaussian random noise, i.e. we compute $d^\eta = d + \eta$ with $\eta \sim N(0, \Gamma)$. We assume the error covariance matrix Γ discussed in the previous section is diagonal with elements equal to the variance of each of the measurements. The standard deviation for pressure measurement errors is 200 Pa. Measurement errors for front location are 2% of the size of the (noise-free) measurements.

We use virtual measurements d^η to infer $\varphi^\dagger(x)$ and $K^\dagger(x)$ within the Bayesian approach discussed in subsection 2.3. We select a prior for $u(x) = (\varphi_1(x), \varphi_2(x), \kappa_1(x), \kappa_2(x), \xi(x))$ as described in Appendix B. We generate an initial ensemble of $J = 120$ particles and compute the corresponding ensemble of

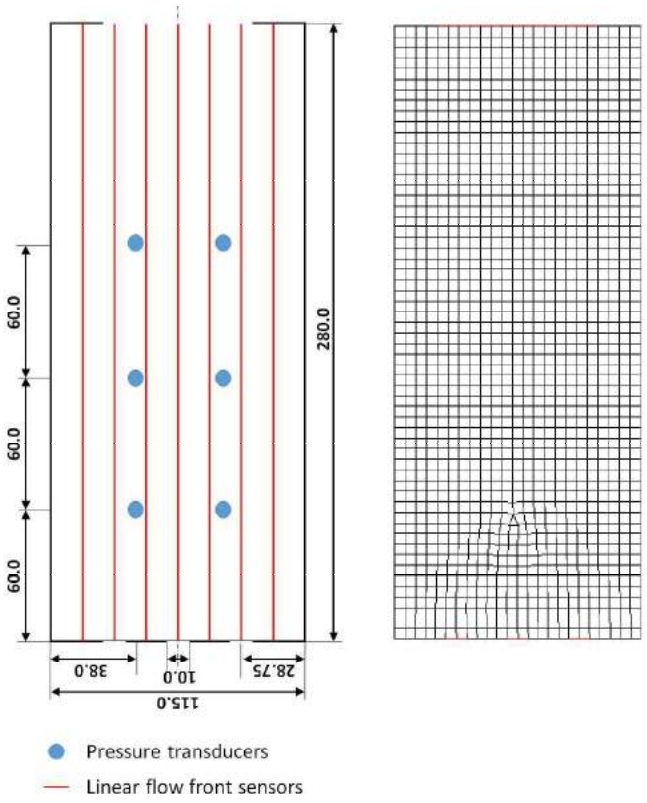

Figure 3: Geometry of the rectangular tool and the corresponding mesh.

permeability and porosity (e.g. via using the initial ensemble in formulas analogous to (2.20)). Some samples of the prior ensembles for porosity and permeability are displayed in Fig. 5 (left). The prior mean and variance of these ensembles are displayed in Fig. 6 (top). With this selection of priors, we account for substantial variability in the underlying parameter u which is, in turn, reflected in variability in porosity and permeability. Moreover, from Fig. 6 (top) we observe that the mean and variance do not assume the presence of defects. Our prior assumptions on permeability and porosity also result in substantial variability in the uncertainty in the prior predictions of pressure and flow front locations. Some of these measurements are displayed in the top panels of Fig. 7 (pressure) and Fig. 8 (flow front location).

We now report the results obtained from applying REnKA with the aforementioned selection of a prior ensemble. In Fig. 4 we display the estimate of porosity (middle-right panel) and permeability (right panel) obtained via (2.4)-(2.5), upon convergence of REnKA (after 6 iterations). We can clearly see that the location of the circular defects has been successfully identified. Further validations are provided by the posterior mean and variance of the ensembles of porosity and permeability displayed in Fig. 6 (bottom). While the posterior mean enable us to successfully identify the preform defects, we note that there is relatively large uncertainty (variance) around the interface between background and defects. The variability in the estimates produce by REnKA can also be observed from Fig. 5 (right) where we display some members of the posterior ensemble of porosity (top) and permeability (bottom). Posterior prediction of pressure and front location (at some sensors) are shown in the bottom panels of Fig. 7 (pressure) and Fig. 8 (flow front location). We note that the reduction in the uncertainty in porosity and permeability yields a substantial reduction in the predictions of pressure and front which are, in turn, consistent with the virtual data.

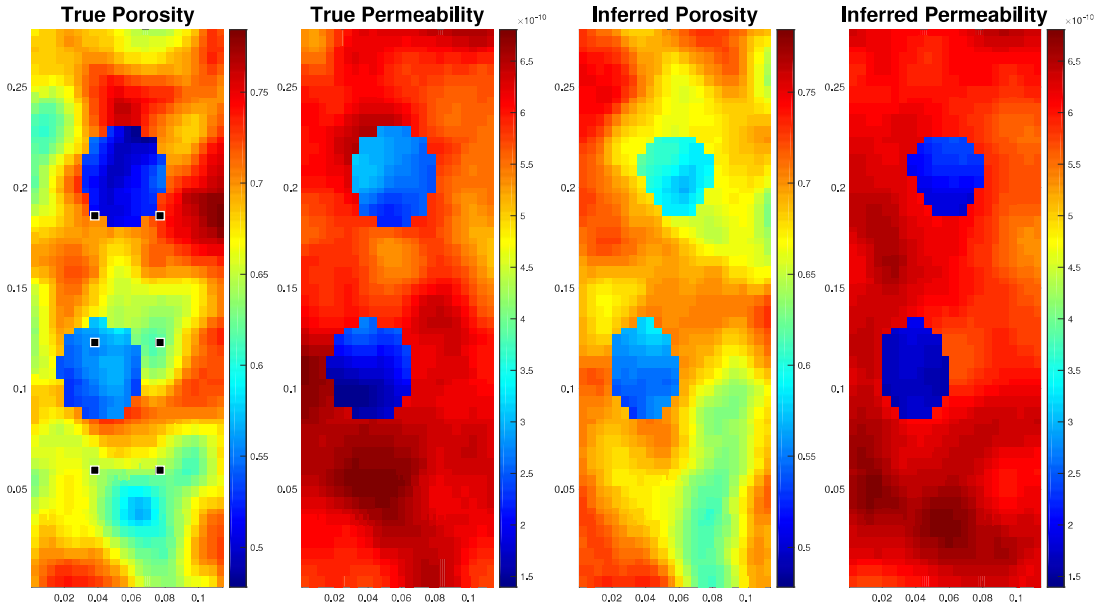

Figure 4: Virtual experiment (rectangular part). Left: True porosity. Left-middle: True permeability. Middle-right: Inferred porosity (via eq. (2.4)). Right: Inferred permeability (via eq. (2.5)).

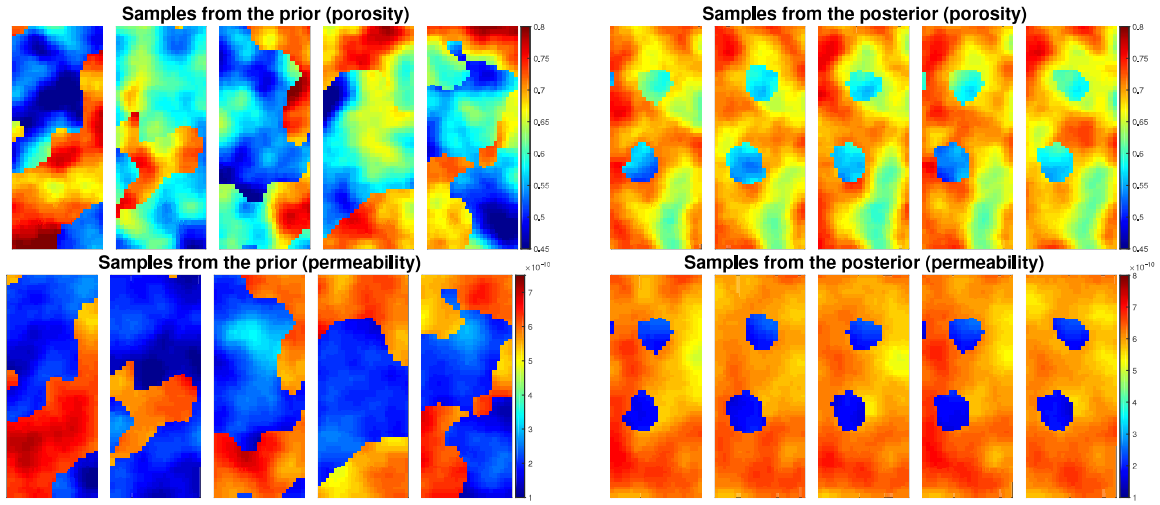

Figure 5: Virtual experiment (rectangular part). Left: Samples from the prior of porosity (top) and permeability (bottom). Right: Samples from the posterior of porosity (top) and permeability (bottom).

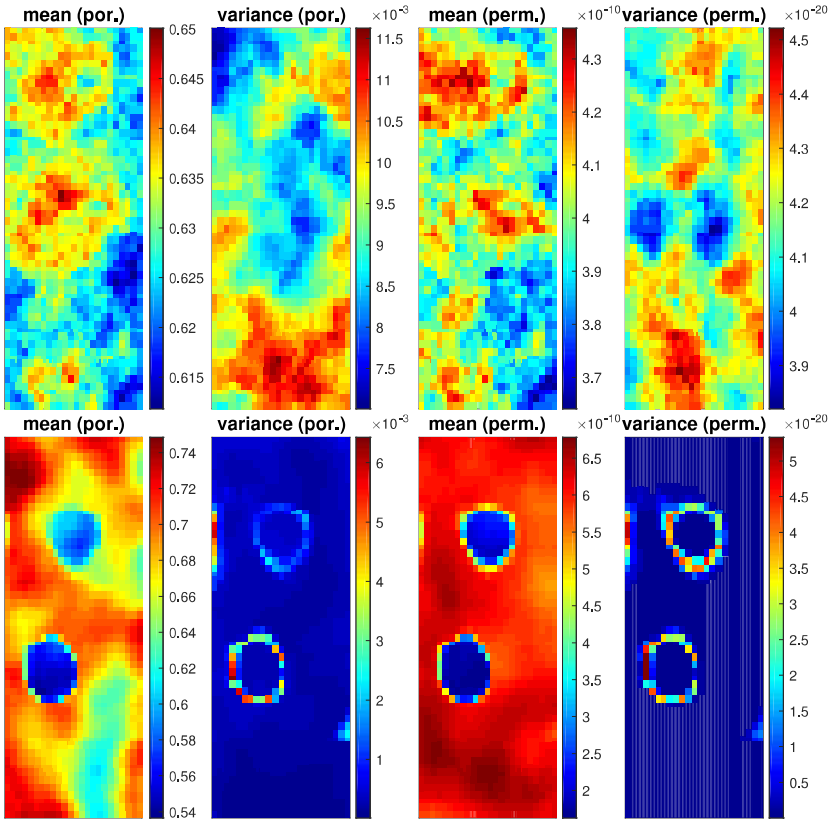

Figure 6: Virtual experiment (rectangular part). Top: Prior mean and variance of porosity and permeability. Bottom: Posterior mean and variance of porosity and permeability.

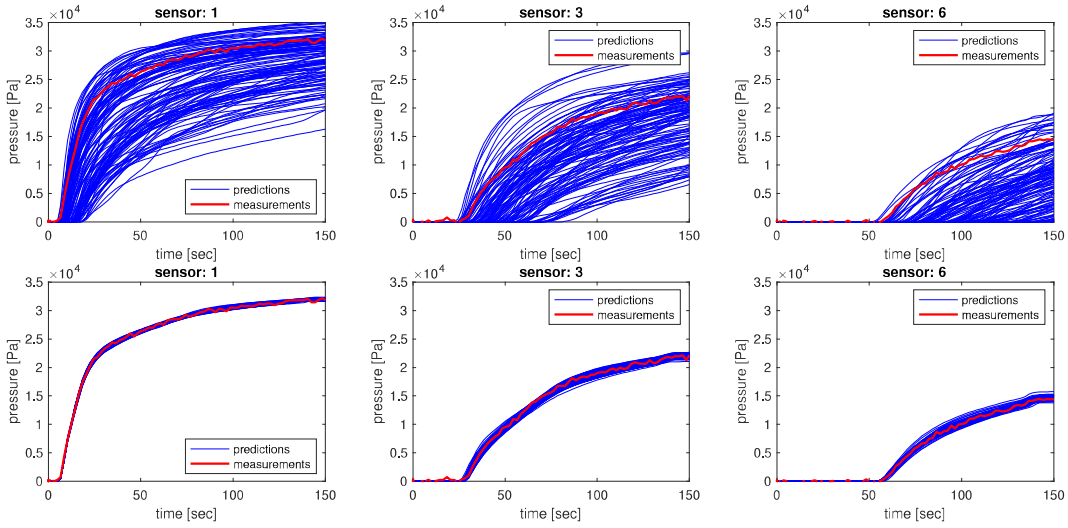

Figure 7: Virtual experiment (rectangular part). Top: Prior predictions of pressure measurements (blue line) and virtual data (red line). Top: Posterior predictions of pressure measurements (blue line) and virtual data (red line).

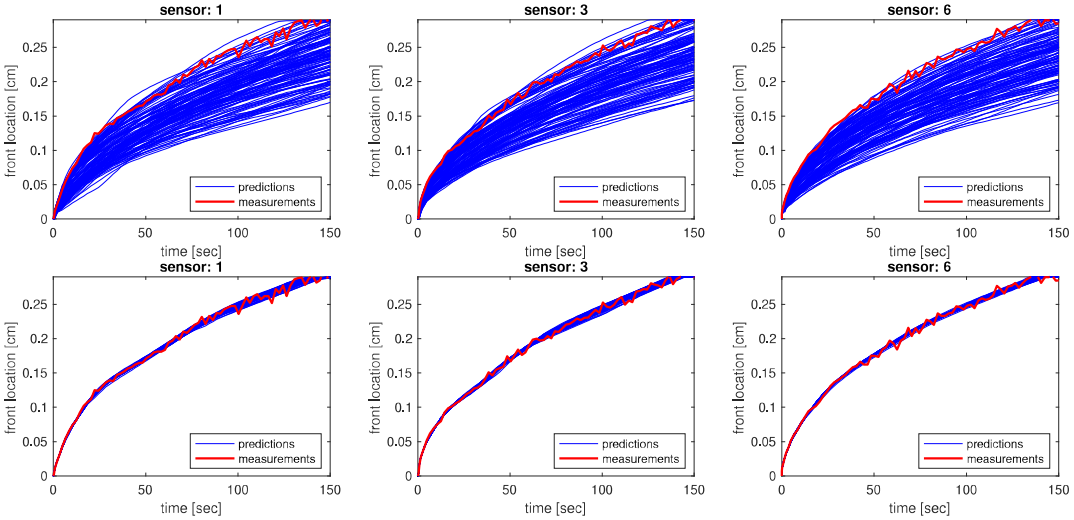

Figure 8: Virtual experiment (rectangular part). Top: Prior predictions of flow front measurements (blue line) and virtual data (red line). Top: Posterior predictions of flow front measurements (blue line) and virtual data (red line).

3.2. Tunnel part

An adapted geometry of an automotive component, namely transmission tunnel, was used to validate REnKA on a more complex 3D problem. The tunnel, shown in Fig. 9(left), has overall dimensions of 0.70 m×0.35 m ×0.15 m and fitted with 267 virtual pressure sensors located approximately on a grid of 0.15 m×0.15 m×0.10 m. Resin flow through the preform is simulated using transient two-phase flow in ANSYS Fluent© under the same assumptions and solver settings as described in subsection 3.1. The pressure at the inlet, located at the narrow end of the tunnel, is set to 1 bar. The pressure at the outlet, located at the wide end of the tunnel, is set to 0 bar. The fluid viscosity is set to 0.1Pa·s.

For validation, we construct the true porosity $\varphi^{\dagger}(x)$, which is shown in Fig. 9(right), with background porosity equal to 0.5 and defects having higher porosity of 0.7. The true permeability $K^{\dagger}(x)$ is then constructed assuming that dependence of permeability on porosity can be expressed as

$$K(x) = a(1 - \varphi(x))^b \tag{3.1}$$

with our choices of $a = 10^{-10}$ m^2 and $b = -1.4$.

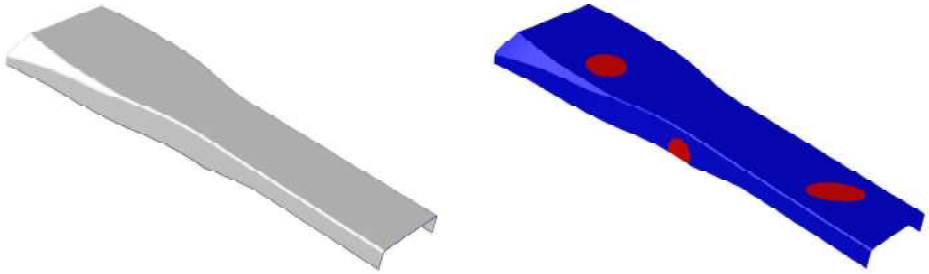

Figure 9: Overall view of the tunnel geometry (left); Porosity defects (in red) in the tunnel preform (right).

Virtual measurements d^{η} are used to infer $\varphi^{\dagger}(x)$ and $K^{\dagger}(x)$ within the Bayesian approach discussed in subsection 2.3. The virtual measurements of pressure are superimposed with 1% noise. The parame-

terisation in this case was via permeability, i.e. $K(x)$ was written as before (see (2.4):

$$K(x) = \kappa_1(x) + (\kappa_2(x) - \kappa_1(x))\mathbb{1}_{A_\xi}(x) \tag{3.2}$$

then κ_1 and κ_2 can be identified. Having $K(x)$, the inferred porosity is computed according to (3.1).

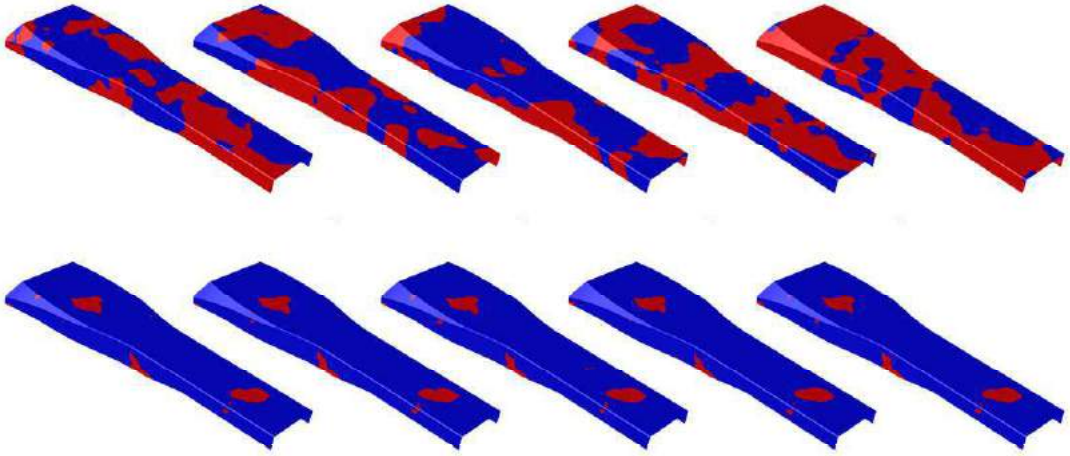

Figure 10: Samples from the prior porosity ensemble (top); Samples from the posterior porosity ensemble (bottom). Red=porosity of 0.7, blue=porosity of 0.5.

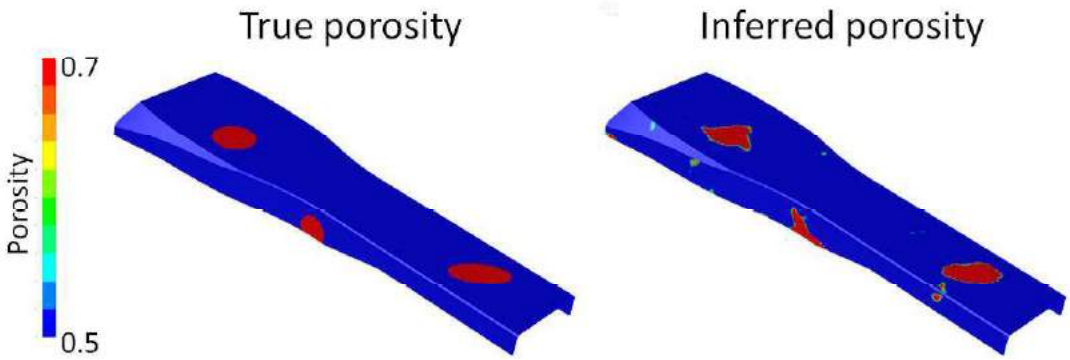

Figure 11: True and inferred porosities.

For simplicity, it is assumed in this experiment that porosity is constant and known for both the defects and background. Therefore, the main objective of this virtual experiment is to identify defect locations only (i.e., underlying level-set function $\xi(x)$ in a 3D domain with complex geometry). The initial ensemble of $J = 100$ particles is generated and used to compute the corresponding ensembles of permeability and porosity. Some samples of the prior ensembles for porosity are shown in Fig. 10(top). This choice of prior does not assume any knowledge of position of defects and has a substantial variability.

Using the described setting, REnKA converged after 7 iterations and produced a posterior ensemble of porosity shown in Fig. 10(bottom). The mean is computed from this ensemble to identify locations of the defects. It is shown in Fig. 11 along with the true porosity $\varphi^\dagger(x)$. It can be seen that the inferred porosity captures all three defects in the preform.

Future virtual experiments with the tunnel will include inferring not only locations of defects but also heterogeneous values of porosity and permeability inside the defects and in the background similar to how it is done in subsection 3.1 for the simple geometry.

4. Validation in a lab experiment

A rectangular mould with three inlet gates and one outlet, with identical configuration to that used in subsection 3.1, was used in the experiments. The mould consists of a steel bottom, a spacer frame of 2 mm thickness and a transparent top. Each of the inlets is connected to a pressure tank fitted with an electro-pneumatic pressure regulator. Six pressure transducers, mounted in the bottom of the mould, are connected to data acquisition equipment to collect the measurements. A digital video camera was used to record the mould filling process and obtain flow front positions.

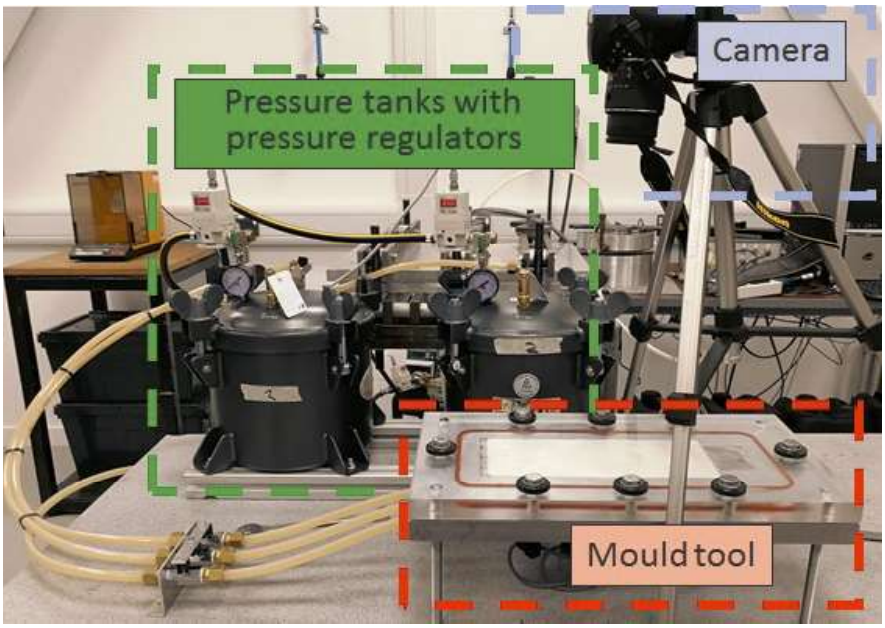

Figure 12: The lab experiment setting.

Figure 13: Defects in the preform.

Continuous glass fibre random mat, Unifilo©, was used for the experiments. The areal weight of the reinforcement was measured to be 259 g/m^2 with a standard deviation of 15 g/m^2. The preforms used

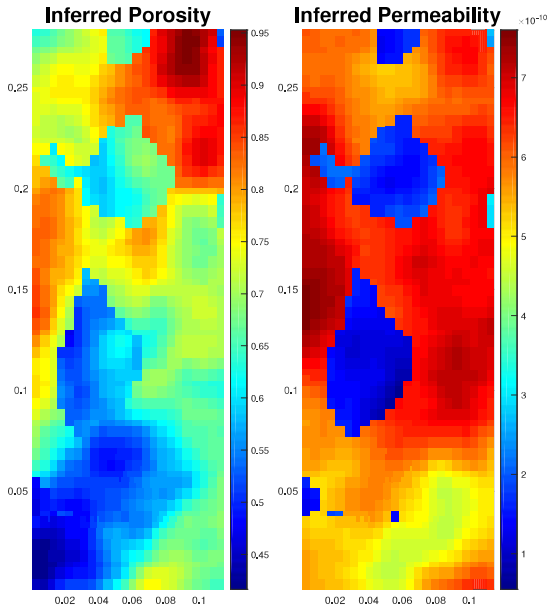

Figure 14: Lab experiment (rectangular part). Left: Inferred porosity (via eq. (2.4)). Right: Inferred permeability (via eq. (2.5)).

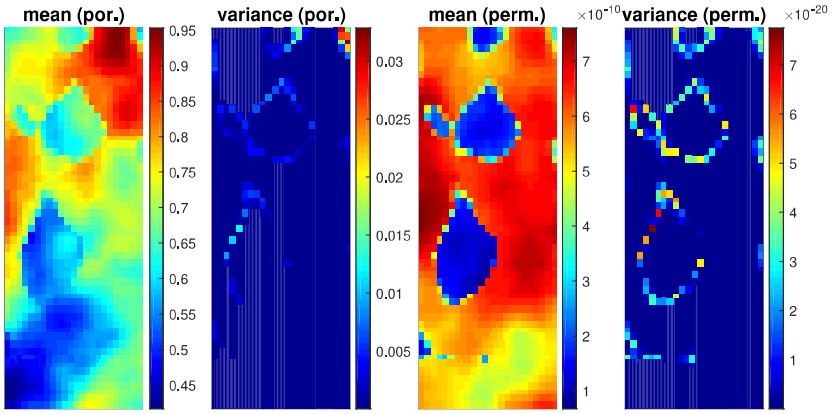

Figure 15: Lab experiment (rectangular part). Posterior mean and variance of porosity and permeability.

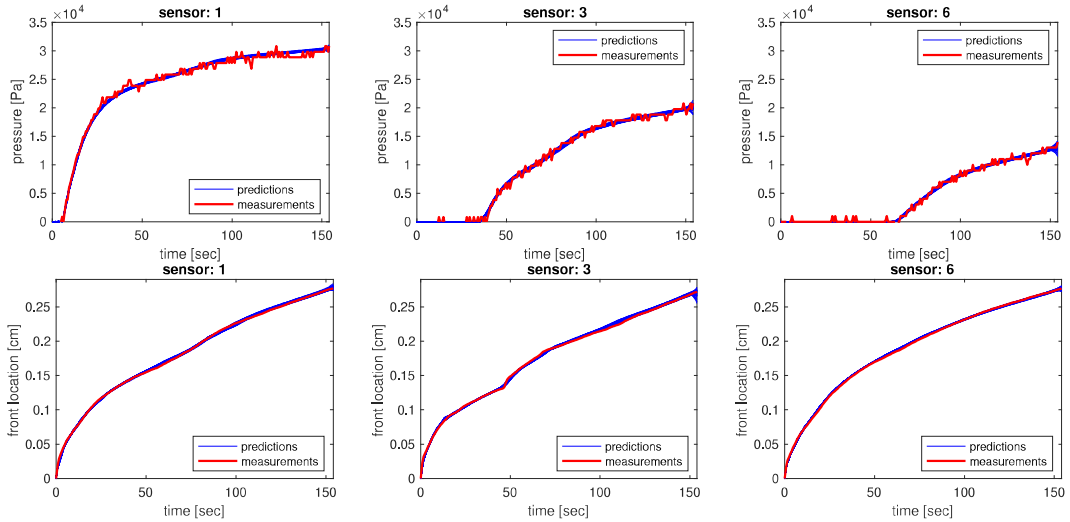

Figure 16: Lab experiment (rectangular part). Posterior predictions (blue line) of pressure (top) and front location; real data are displayed in red line.

in experiments were consisting of 7 layers of the reinforcement compacted to a porosity of approximately 0.71. Defects were created by placing circular patches of additional 4 layers of the reinforcement in the middle of the preform (see Fig. 13) at the positions and of the size described in subsection 3.1. The injection fluid was engine oil at a constant temperature of 19.5°C with a viscosity of 0.106 Pa·s. The injection pressure at all three gates was set to 0.4 bar.

We apply REnKA with the experimental data collected as described earlier. We initialised the algorithm with the same initial ensemble as in subsection 3.1. Based on regression analysis on the lab data, we determine that measurements errors in pressure data have a standard deviation of approximately 300 Pa. Errors in flow front positions are estimated to be approximately 5%. We use this information to construct the error covariance matrix Γ.

REnKA converges after 10 iterations. The posterior ensemble of unknown parameters is used in (2.4)-(2.5) to compute the inferred porosity and permeability. These are displayed in Fig. 14. Posterior mean and variances are shown in Fig. 15. We note that porosity and permeability indicate the presence of defects that were engineered in the lab experiment. We observe that there is unintended variability in porosity and permeability in the background. This variability represents inherent variability of the reinforcement used in the experiments. It was estimated experimentally that the variability of porosity can be up to 10%. Nevertheless, from Fig. 16 we note that the posterior predictions of pressure and flow front show that an excellent fit to the data has been achieved.

5. Conclusions

We applied a novel Bayesian inversion algorithm to RTM processes. In virtual and lab experiments, we demonstrated that the algorithm can successfully identify material defects via the estimation of regions of high contrast in porosity and permeability. The algorithm also provides a measure of uncertainty (via variance) which is relatively large at the interface between background and defects. For real experiments, we showed that the algorithm can recover defects albeit with a lower degree of accuracy compared to virtual experiments. Possible reasons are (i) experimental data is affected by larger errors which are detrimental to the algorithm, (ii) modelling errors which are larger than measurement errors produce bias estimates. This is the first step in using in-process data and the Bayesian inversion methodology to

improve and speed up NDE of composites parts, which in turn will deliver more robust, more reliable and cheaper manufacturing of composites.

Future work will include incorporation of better prior models and/or infer the prior within the Bayesian inversion algorithm [10, 16]. Further testing is required in both virtual and lab experimental settings. In the former, more testing is needed for complex geometry allowing for permeability and porosity to be heterogeneous inside and outside defects as it was done here in the case of simple flat geometry and also to have defects of significantly different shapes. Lab experiments with more complex geometry need to be conducted. Furthermore, the success of in-process data collection and hence of estimating properties of produced composites parts depends on quality and resolution of pressure and/or arrival sensors which should be developed further and become cheaper for the digital revolution in composites manufacturing to succeed.

[1] Endruweit, A. and A.C. Long. Infuence of stochastic variations in the fibre spacing on the permeability of bi-directional textile fabrics. Composites Part A. 37 (5): 679-694, 2006.

[2] Endruweit, A. and A.C. Long, F. Robitaille, C.D. Rudd. Influence of stochastic fibre angle variations on the permeability of bi-directional textile fabrics. *Composites A* 37: 122-32, 2016

[3] Mesogitis, T.S., A.A. Skordos, and A.C. Long. Uncertainty in the manufacturing of fibrous thermosetting composites: a review. Composites Part A. 57: 67-75, 2014.

[4] Matveev, M.Y., F. Ball, I.A. Jones, A.C. Long, P.J. Schubel, and M.V. Tretyakov. Uncertainty in geometry of fibre preforms manufactured with Automated Dry Fibre Placement (ADFP) and its effects on permeability. J. Composite Materials. 52(16): 2255-2269, 2018.

[5] Padmanabhan, S.K. and R. Pitchumani. Stochastic modelling of nonisothermal flow during resin transfer molding. Int. J. Heat Mass Trans. 42: 3057-3070, 1999.

[6] Park, M. and M.V. Tretyakov. Stochastic resin transfer molding process, SIAM/ASA J. Uncertainty Quantification. 5: 1110-1135, 2017.

[7] https://www.compositesworld.com/blog/post/zero-defect-manufacturing-of-composite-parts

[8] Iglesias, M.A., M. Park, and M.V. Tretyakov. Bayesian inversion in resin transfer molding. Inverse Problems. 34(10): 1005002, 2018.

[9] Iglesias, M.A., Y. Lu and A.M. Stuart. A Bayesian level let method for geometric inverse problems. Interfaces and Free Boundaries. 18: 181-217, 2016.

[10] Dunlop, M. M., M. A. Iglesias and A.M. Stuart. Hierarchical Bayesian level set inversion. Statistics and Computing. 27: 1555-1584, 2017.

[11] Stuart, A.M. Inverse problems: a Bayesian perspective. Acta Numerica. 19: 451 - 559, 2010.

[12] Kantas, N., A. Beskos and A. Jasra. Sequential Monte Carlo Methods for High-Dimensional Inverse Problems: A Case Study for the Navier–Stokes Equations. SIAM/ASA J. Uncertainty Quantification. 2(1): 464-489, 2014.

[13] Wei, B.-J., Y.-S. Chang, Y. Yao and J. Fang. Online estimation and monitoring of local permeability in resin transfer molding. Polymer Composites. 37: 1249-1258, 2016.

[14] Caglara, B., D. Salvatori, E.M. Sozer and V. Michaud. In-plane permeability distribution mapping of isotropic mats using flow front detection. Composites Part A. 113: 275-286, 2018.

[15] Lasanen, S., M. J. Huttunen and L. Roininen. Whittle-Matérn priors for Bayesian statistical inversion with applications in electrical impedance tomography. Inverse Problems and Imaging. 2(8): 561-586, 2014.

[16] Chada, N. K., M. A. Iglesias, L. Roininen and A.M. Stuart. Parameterizations for ensemble Kalman inversion. Inverse Problems. 34(5): 055009,2018.

[17] Advani, S.G. and E.M. Sozer. Process Modeling in Composites Manufacturing. CRC Press, 2010.

[18] , Lord, G. J., C. Powell and T. Shardlow. An introduction to computational stochastic PDEs. Cambridge University Press, 2014.

Acknowledgments

This work was supported by the Engineering and Physical Sciences Research Council [grant number EP/P006701/1]; through the EPSRC Future Composites Manufacturing Research Hub.

Appendix A. Resin Infusion Model

We now describe the forward model (see further details in [6, 8, 17]). Let $D^* \subset \mathbb{R}^d$, $d \in \{1, 2\}$, be an open domain representing a physical domain of a porous medium with the permeability $\kappa(x)$ and porosity φ. The boundary of the domain D^* is $\partial D^* = \partial D_I \cup \partial D_N \cup \partial D_O$, where ∂D_I is the inlet, ∂D_N is the perfectly sealed boundary, and ∂D_O is the outlet. The domain D^* is initially filled with air at a pressure p_0. This medium is infused with a fluid (resin) with viscosity μ through an inlet boundary ∂D_I at a pressure p_I and moves through D^* occupying a time-dependent domain $D(t) \subset D^*$, which is bounded by the moving boundary $\Upsilon(t)$ and the appropriate parts of ∂D.

The forward problem for the pressure of resin $p(t, x)$ consists of the conservation of mass

$$\nabla \cdot \mathbf{v} = 0, \qquad x \in D(t),\ t > 0, \tag{A.1}$$

where the flux $\mathbf{v}(x, t)$ is given by Darcy's law

$$\mathbf{v}(x, t) = -\frac{\kappa(x)}{\mu} \nabla p(x, t) \tag{A.2}$$

with the following initial and boundary conditions

$$\begin{aligned}
p(x,t) &= p_I,\ x \in \partial D_I,\ t \geq 0, && \text{(A.3)}\\
\nabla p(x,t) \cdot \mathbf{n}(x) &= 0,\ x \in \partial D_N,\ t \geq 0, && \text{(A.4)}\\
V(x,t) &= -\frac{\kappa(x)}{\mu\varphi(x)} \nabla p(x,t) \cdot \mathbf{n}(x,t), \quad x \in \Upsilon(t),\ t \geq 0, && \text{(A.5)}\\
p(x,t) &= p_0,\ x \in \Upsilon(t),\ t > 0, && \text{(A.6)}\\
p(x,t) &= p_0, x \in \partial D_O,\ t > 0, && \text{(A.7)}\\
p(x,0) &= p_0,\ x \in D^*, && \text{(A.8)}\\
\Upsilon(0) &= \partial D_I. && \text{(A.9)}
\end{aligned}$$

Here $V(x, t)$ is the velocity of the point x on the moving boundary $\Upsilon(t)$ in the normal direction at x, $\mathbf{n}(x)$ and $\mathbf{n}(x, t)$ are the unit outer normals to the corresponding boundaries.

We consider N_p pressure sensors at locations denoted by $w_i^p = (x_i^p, y_i^p)$, $i = 1, \ldots, N_p$, and N_f linear sensors with coordinates defined via the sets $\mathcal{F}_i = \{(x, y) \in D | x = x_i^f, y \in [0, L]\}$, $i = 1, \ldots, N_f$. Let $y_i^f(t)$ be such that

$$(x_i^f, y_i^f(t)) \equiv \mathcal{F}_i \cap \Upsilon(t).$$

In other words, $y_i^f(t)$ is the y-coordinate of the position of the flow front measured at the ith linear sensor. We are interested in monitoring pressure at sensors locations as well as the flow front location

(measured at linear sensors) at a collection of N_t observation times $\{t_m\}_{m=1}^{N_t}$. At each observation time t_m, we combine all measurements of pressure and flow front in the following variable

$$d = \big(\{p(w_i^p, t_1)\}_{i=1}^{N_p}, \ldots, \{p(w_i^p, t_{N_t})\}_{i=1}^{N_p}, \{y_i^f(t_1)\}_{i=1}^{N_f}, \ldots, \{y_i^f(t_{N_t})\}_{i=1}^{N_f}\big). \tag{A.10}$$

We note that for specified μ, p_0 and p_I, the resin injection model (A.1)-(A.9), together with measurement predictions defined in (A.10) induced a map

$$d = \mathcal{F}(\kappa, \phi),$$

that maps porosity and permeability into model predictions of pressure and flow front at sensor locations and specified observation times during the simulation of resin injection.

Appendix B. The Prior

As we discussed in subsection 2.3, the Bayesian approach enables us to incorporate prior knowledge of the unknown parameters $u(x) = (\varphi_1(x), \varphi_2(x), \kappa_1(x), \kappa_2(x), \xi(x))$ that we wish to infer. In this subsection we discuss our selection of the prior distribution for these variables. We recall that samples from these priors are needed in order to generate the initial ensemble that we must specify to initialise Algorithm 1.

For simplicity, let us first assume that, under the prior, the unknown parameters $\varphi_1, \varphi_2, \kappa_1, \kappa_2, \xi$ are independent random functions and so the joint prior can be written as

$$\mathbb{P}(u) = \mathbb{P}(\varphi_1, \varphi_2, \kappa_1, \kappa_2, \xi) = \mathbb{P}(\varphi_1)\mathbb{P}(\varphi_2)\mathbb{P}(\kappa_1)\mathbb{P}(\kappa_2)\mathbb{P}(\xi), \tag{B.1}$$

where $\mathbb{P}(\varphi_1)$, $\mathbb{P}(\varphi_2)$, $\mathbb{P}(\kappa_1)$, $\mathbb{P}(\kappa_2)$ and $\mathbb{P}(\xi)$ are the priors of φ_1, φ_2, κ_1, κ_2, and ξ, respectively. In a practical context, our prior knowledge (e.g. from previous experiments) of these parameters could suggest correlations between these parameters; these correlations can be incorporated within the proposed framework.

	φ_1	φ_2	κ_1	κ_2	ξ
ν	1.85	1.85	1.85	1.85	2.5
l [cm]	1.183×10^{-2}	1.183×10^{-2}	1.183×10^{-2}	1.183×10^{-2}	2.2×10^{-2}
σ^2	0.05	0.05	1.6×10^{-21}	1.6×10^{-21}	1
mean*	0.55	0.71	2×10^{-10}	6×10^{-10}	0

Table B.1: Prior parameters. *prior means were assumed constant.

In order to define priors for the functions φ_1, φ_2, κ_1, κ_2, and ξ, we propose the use of Gaussian random fields [18]. Our aim is to use Gaussian priors to characterise, via a wide class of functions, the spatial variability in the material properties. We assume that, under the prior, each of the functions φ_1, φ_2, κ_1, κ_2, and ξ are stationary Gaussian random functions/fields (GRF) with a prescribed mean covariance operator induced by the Whittle-Mattern covariance function given by [15]:

$$f_{\sigma,\nu,l}(x, y) = \sigma^2 \frac{2^{\nu-1}}{\Gamma(\nu)} \left(\frac{|x-y|}{l} \right)^{\nu} K_\nu \left(\frac{|x-y|}{l} \right), \tag{B.2}$$

where $\nu > 0$ is a parameter that controls the regularity/smoothness of the samples, l is the characteristic length scale, σ_κ^2 is the variance, Γ is the gamma function, and K_ν is the modified Bessel function of the second kind of order ν. In Table B.1. we display the selection of mean and parameters in the Whittle-Mattern covariance function (B.2) for each of the functions φ_1, φ_2, κ_1, κ_2 and ξ. It is important to mention that the selection of the prior variance σ for each of the parameters φ_1, φ_2, κ_1, κ_2 has been made so that the resulting samples are positive with very high probability. We reiterate that the prior means reflect our prior knowledge of these quantities according to the design. The generation of a random functions from such a distribution can be achieved by means of the Karhunen-Loeve (KL) expansion [18].

.

Part II: Algorithms for active control of resin infusion in RTM process with uncertainties

M.Y. Matveev[a], A. Endruweit[a], A.C. Long[a], M.A. Iglesias[b], M.V. Tretyakov[b]

[a]*Composites Group, Faculty of Engineering, University of Nottingham, Nottingham, UK*
[b]*School of Mathematical Sciences, University of Nottingham, Nottingham, UK*

Abstract

An active control system (ACS) aimed at reducing deviations of a real RTM process influenced by random disturbances from the expected (reference) process according to a design is developed. Using a very fast pseudo-1D Bayesian inverse algorithm, the ACS estimates permeability and porosity based on which it then computes new pressure values on the inlets required to have the flow front position at the next observation time to match the reference position of the front within the tolerance level. The ACS is tested in both virtual and lab experiments confirming its feasibility.

Keywords: Resin transfer moulding, random permeability and porosity, Bayesian inverse algorithms, stochastic control, uncertainty quantification.

1. Introduction

Resin Transfer Moulding (RTM) process is an attractive way of producing composite materials due to its versatility. But the use of RTM (especially, in the case of aerospace application which have very low tolerance to defects in produced parts to ensure their safety of use) is hindered by its substantial irreducible uncertainties and variabilities [1–3]. The variability can lead to incomplete mouldings and to not having a repeatable mould filling process with minimum deviations from the design. Such deviations typically cause dry spots and/or high micro-void content. Here we propose an active control system (ACS) aimed at reducing deviations from the designed process.

A number of attempts have been made to develop control systems, see e.g. [4–6] and references therein. In [4] a control system exploits a surrogate model such as artificial neural network. Surrogate models are not physics-based and their performance degrades when they encounters cases which are significantly different from those used for the model training. They require extensive (usually highly computationally demanding) training before they can be used, and this training needs to be repeated for any new design of the process. In contrast, the ACS presented in this paper uses a physics-based resin injection model which can work online for a real mould filling process without any prior training and it can deal with any new scenario automatically. In comparison with [5, 6], the presented ACS exploits an efficient, novel Bayesian inversion (BI) algorithm (REnKA from [7], see also [8]) for estimation of local permeability and porosity to have more accurate control.

In this paper, we test the feasibility of such an ACS in terms of computational time required for the ACS algorithm as well as its ability to reduce the error compared to an uncontrolled RTM process. These will be verified in virtual and physical experiments.

Email addresses: Mikhail.Matveev@nottingham.ac.uk (M.Y. Matveev), Andreas.Endruweit@nottingham.ac.uk (A. Endruweit), Andrew.Long@nottingham.ac.uk (A.C. Long), Marco.Iglesias@nottingham.ac.uk (M.A. Iglesias), Michael.Tretyakov@nottingham.ac.uk (M.V. Tretyakov)

This second part of the report is organised as follows. The ASC is described in Section 2 with technical details given in Appendices. Results for virtual experiments are presented in Section 3. The test conducted in the lab is considered in Section 4. The last section contains discussions and conclusions.

2. Active control system (ACS)

The ACS is aimed at controlling flow patterns during impregnation of a fibrous preform with a resin. It requires that a resin injection simulation for the considered part with its designed parameters was performed on a space-time grid prior to the use of ACS, and that the result of this simulation is recorded in terms of positions of the flow front on the time grid. This result is called 'flow according to the design' throughout the text. The objective of ACS is to minimise deviation of the flow front positions under real conditions from the front positions according to the design. It is assumed that deviations from the design occur because of local variability of permability and porosity caused by heterogeneity of preforms, while other variabilities such as resin viscosity or fluctuations of injection pressure at the inlets are neglected.

The ASC has the following schematic structure. For a selected distance (e.g. maximum deviation) a tolerance level for deviation of the flow front positions under real conditions from the front positions according to the design is selected. On a pre-determined time grid and at every time step the algorithm does the following.

1. Compute the distance between the current flow front position and the front position according to the design as it should be at this time.
2. If the distance is smaller than the set tolerance, do not perform any further actions.
3. If the distance is larger than the tolerance then
   (a) Estimate permeability and porosity using a BI algorithm given the data from pressure and flow front sensors collected from the start of resin injection until the current time.
   (b) Compute the pressure values at each of the injection gates using the estimated local permeability and porosity so that at the next time point of the grid the distance between the current flow front position and the front position according to the design is minimised.
   (c) Change pressure on the inlets according to the result of b) and Exit this algorithm.

The steps 3a and 3b rely on a mathematical model of resin infusion process. In this study, a simplified model in the form of pseudo-1D flow is used. The problem formulation, its solution and the approach for finding new pressure on an inlet provided that permeability and porosity have been estimated are given in Appendix A. REnKA from [7] (see also [8]) is used as the BI algorithm required in 3a. It is expected that the use of the pseudo-1D flow together with independent evaluation of pressure on each gate in the ACS can be adequate for an anisotropic material with permeability in the direction of the flow significantly (by a factor of 10 or more) dominating the transverse permeability. For the case of isotropic permeability influence on pseudo-1D flow from neighbouring gates cannot be ignored. The required correction is described in Appendix B.

The BI algorithm used in step 3a was implemented in C and built into a DLL library for linking to an external program. The implementation was optimised to run REnKA in 1-2 seconds depending on the amount of data and precision of required predictions. Moreover, a simplified deterministic version of step 3a with an execution time of 0.25s was implemented as well. The deterministic algorithm assumed that the permeability and porosity are constant (but not known) and can be computed from single measurement of the flow front position and pressure history at a particular time step. These two implementations are sufficiently fast to be used in a realistic ACS.

3. Validation with virtual experiments

In this section we describe virtual experiments for testing the ACS from Section 2. Note that we used a similar setting for one of the virtual experiments in Part I of the report [8].

3.1. Virtual experiment setup

A number of tests of the proposed ACS and its algorithm were performed using virtual experiments. Flow through a porous reinforcement in a rectangular mould was simulated using a transient two-phase flow model within ANSYS Fluent©. It was assumed that the permeability of the reinforcement does not change with time (no compaction or decompaction, no change of properties with saturation) but can vary from point to point. The viscosity of the fluid remained constant (i.e., the proccess is assumed to be isothermal with no resin cure present). No-slip boundary conditions were imposed at the walls of the cavity. Boundary conditions at the inlets and outlets are pressure boundary conditions. Finally, the model was assumed to neglect any through-thickness effects which made it possible to use a 2D implementation of the numerical algorithm. The permeability is assumed to stay constant within an element of the mesh used in simulations but can vary in between the elements. The latter case is implemented via user-defined functions (UDF) written in C which make it possible to extend ANSYS Fluent© capabilities. The Fluent solver settings were: pressure-based solver; implicit VOF formulation; SIMPLE algorithm for pressure-velocity coupling; spatial discretisation of gradient using Green-Gauss Node Based gradient method; spatial discretisation of pressure and momentum using PRESTO! and third-order MUSCL methods, discretisation of volume fraction using modified HRIC method. Under-relaxation and convergence settings were kept to their default values.

A schematic drawing of a rectangular mould with three inlet gates and one outlet is shown in Fig. 1. Six pressure sensors and seven equally spaced linear flow sensors are placed within the tool. Mesh convergence studies were performed for a case with constant inlet pressure applied to all three gates. The resulting mesh of the geometry is shown in Fig. 2.

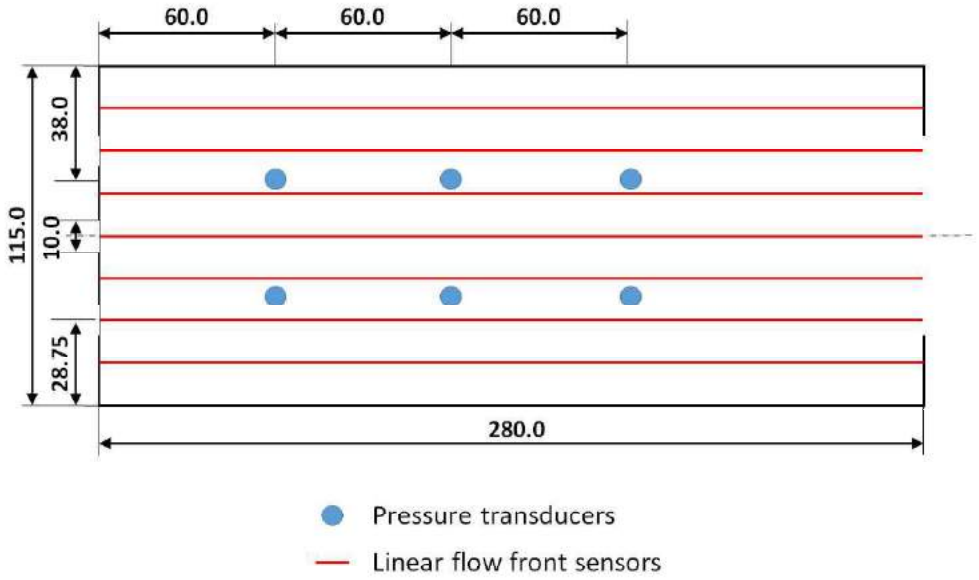

Figure 1: Geometry of the rectangular moulding tool and position of the sensors.

The design case for this configuration was assumed to be impregnation of an isotropic reinforcement with no variability or defects. The nominal porosity of the preform is 0.71 and its permeability is assumed to be isotropic and equal to 5.66×10^{-10} m^2. The fluid viscosity is 0.106 Pa·s. The predicted filling time for the design configuration was 107s at constant injection pressure of 0.4 bar at all three inlets. Readings from the flow front sensors, obtained during the design experiments, are used as an input for the control algorithm ('flow according to the design').

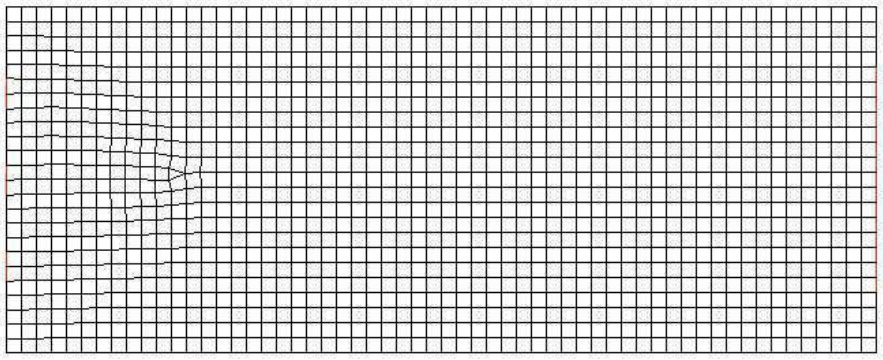

Figure 2: 2D mesh of the geometry of the rectangular moulding tool.

3.2. Controlled and uncontrolled fillings of preforms with defects

The control algorithm outlined in Section 2 was implemented via a user-defined function (UDF) which is executed at the end of each computational time step. The UDF was linked to the DLL containing the BI algorithm [7, 8]. Input of the control algorithm was the data from the 'flow according to the design' and parameters of the nominal infusion such as nominal porosity, permeability and fluid viscosity. The algorithm predicted pressure values at each of the gates which were then varied accordingly. Unlike the complex priors used in [8], the prior used for the ACS was a Gaussian distribution of the permeability and porosity around their nominal values.

The test case for the algorithm was a reinforcement with a severe defect (a rectangular hole of 4 cm×8 cm) located 3 cm away from the inlet as shown in Fig. 3. The defect was modelled as an area with porosity equal to 0.99 and permeability equal to 3×10^{-7} m^2. The permeability of the reinforcement was modelled with local randomness of 10% in both permeability and porosity. The uncontrolled filling was 103 s which is not significantly different from the filling according to the design. The presence of the defect distorted the flow front as shown in Fig. 4. The filling time in the controlled injection was within 108 s which is almost exactly as the design filling time.

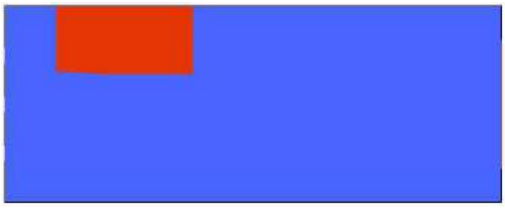

Figure 3: Visualisation of defect in preform used in numerical simulations.

The effectiveness of the controlled filling can be measured via deviations of the actual flow front as detected by the linear flow front sensors from the flow front according to the design $\Delta y_i = y_{design,i} - y_{actual,i}$. The controlled and uncontrolled filling were compared in terms of the maximum deviation of the flow front from the design, i.e. $max(|\Delta y_i|)$. The comparisons are shown in Fig. 5. The controlled filling was performed using deterministic and stochastic algorithms. While, eventually, the flow front was within the tolerance (1 cm) of the flow according to the design, the uncontrolled filling was the slowest to come within this tolerance. The stochastic control algorithm was fastest to reduce the difference between the actual flow and the flow according to the design. However, it was observed that the control algorithms have a higher peak of the maximum deviation when compared to the uncontrolled filling.

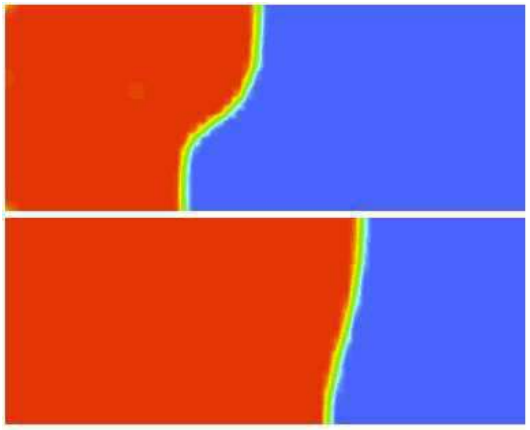

Figure 4: Flow front in uncontrolled filling at 17 s (top) and 38 s (bottom) from the start of the experiment.

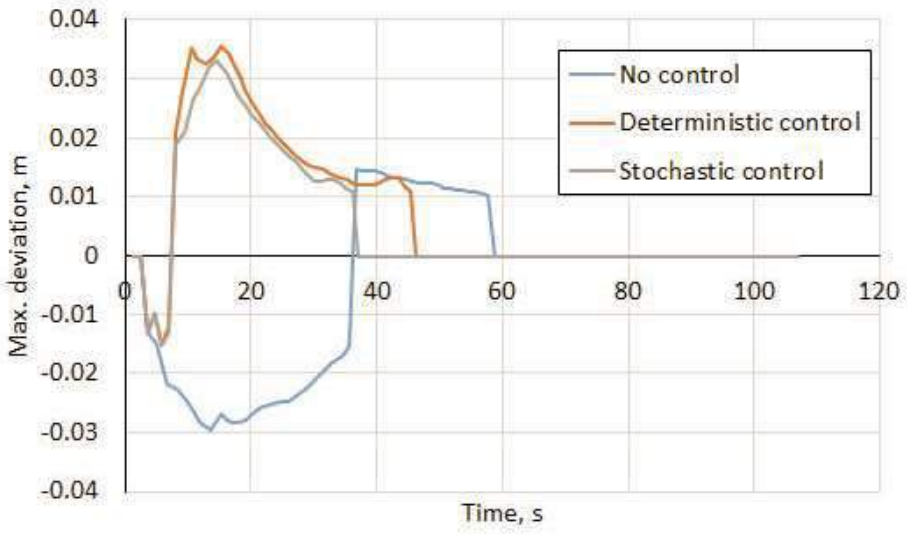

Figure 5: Maximum (in amplitude) deviation of the flow front from the flow according to the design for three types of the filling - uncontrolled, controlled with deterministic algorithm and controlled with stochastic algorithm. The negative sign means that the actual front is ahead of the one according to the design and positive means the opposite.

The results of the virtual experiments showed that the proposed ACS can be feasible not only in terms of being able to control the filling but also in terms of its speed (the control algorithm takes just up to 2 s to be executed) which makes it realistic to be extended to more complex scenarios.

4. Experimental validation

In this section, testing of the ACS in the lab is reported. In subsection 4.1, the experimental setting is described, and in subsection 4.2, results of the tests are given.

4.1. Experimental setup

The rectangular mould with three inlet gates and one outlet, as shown in Fig. 1, was used in the experiments. The mould consists of a steel bottom, a spacer frame of 2 mm thickness and a transparent top. Each of the inlets is connected to a pressure tank fitted with an electro-pneumatic pressure regulator which can be digitally controlled to change pressure in the tank. Non-return valves were fitted to each of the inlet gates to prevent backflow of fluid when pressure at some of the gates is higher than pressure at the other gates. Seven linear flow front sensors were embedded into the mould top. The flow front sensors are based on measuring the resistance of the fluid between two wires [9, 10]. The flow sensors and pressure regulators are connected to a NI-6229 data acquisition board which makes it possible to collect the measurements as well as send the control signals to the pressure regulators. In addition to this equipment, a digital video camera was used to record the mould filling for the further post-processing and analysis of the process. An overall view of the experimental setup is shown in Fig. 6.

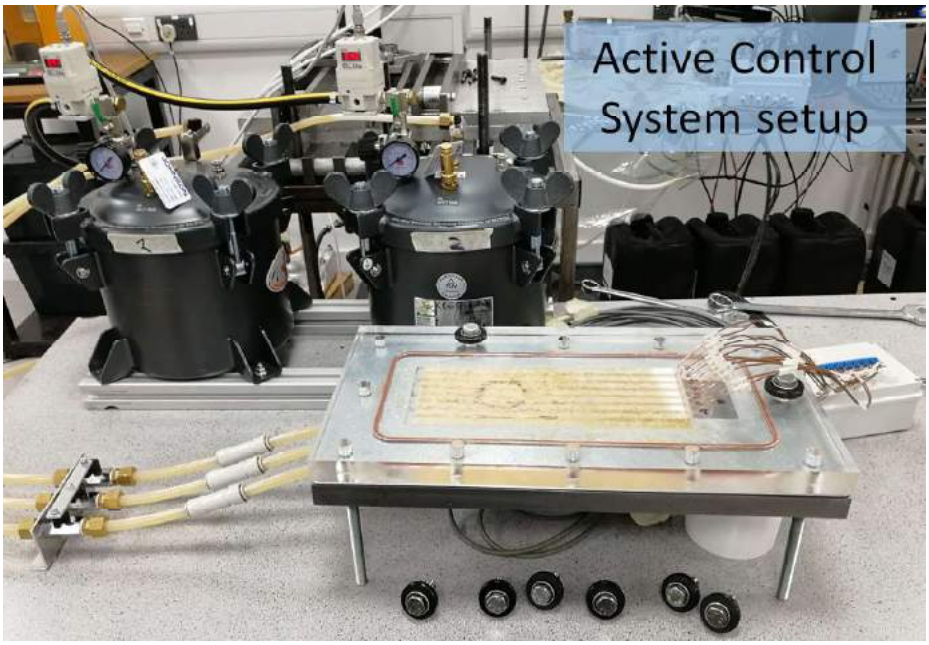

Figure 6: Overall view of the experimental rig for validation of the ACS concept.

The algorithm defined in Section 2 was programmed within the LabVIEW environment and linked to the DLL containing the BI algorithm. The interface of the LabVIEW program included interactive controls of the control algorithm such as time step.

It should be noted that, while in theory voltage readings from the linear flow front sensors can be calibrated and converted to the flow front positions, it is a difficult task for an array of such sensors due

to interactions between them. The measurement error of the linear sensors was estimated to be about ± 3 cm which can be attributed to variations of resistivity of the oil and reinforcement. However, these sensors are still used in this work due to the absence of any other cheap techniques which can collect comparable amount of data. The readings are to be considered a characteristic voltage signature for each injection experiment rather than a quantitative description of the flow front shape. Nonetheless, the voltage signatures can still be used in ACS.

Continuous glass fibre random mat, Unifilo©, was used for the experiments. The areal weight of the reinforcement was measured to be 259 g/m^2 with a standard deviation of 15 g/m^2. The average permeability at a porosity of 0.69 was measured to be 6.15×10^{-10} m^2 with a variability of about 10%. The injection fluid was engine oil at a constant temperature of 19.5°C with a viscosity of 0.106 Pa·s. The experiments on a preform consisting of 7 layers of the material with no defects and overall porosity of 0.71 showed that the mould filling time is 132s at a constant pressure of 0.4 bar applied at all three inlet gates.

It was found that the design simulations are close to that observed with a camera in the lab experiments but do not match well the readings from the flow front sensors due to difficulty of their calibration. Therefore, it was decided to use the results obtained from these experiments as 'flow according to the design' input for the control algorithm.

4.2. Controlled and uncontrolled fillings of preforms with defects

Preforms with a severe defect, a rectangular hole of 4 cm×8 cm located 3 cm from the inlet side as shown in Fig. 7, were used for the experiments. Stages of uncontrolled and controlled fillings of a preform with the defect are shown in Fig. 8. It can be seen that the flow front is distorted by the defect but becomes more or less straight towards the end. However, the filling time was 90 s which is 32% shorter than for the preform with no defect. Controlled filling was performed for the preforms with the same defect. The control time step was selected to be 2 s. The filling time for controlled filling was 116 s which is within 10% of the design filling time.

Figure 7: Overall view of the experimental rig for validation of the ACS concept.

Absence of the in-process pressure readings prevented the stochastic control from being robust. Therefore, only the deterministic control algorithm was used in experiments. However, since the stochastic filling performed better in the virtual experiments, it is expected that results of the deterministic control algorithm will show the potential improvement of a controlled filling over uncontrolled filling.

The maximum deviation of the flow front from the flow according to the design is shown in Fig. 9. It can be seen that the maximum deviation from the design is higher for the uncontrolled filling. A similar peak of the maximum deviation for the controlled filling was observed in the virtual experiments. It also should be noted that the error of the flow front sensors is about ± 3 cm which is comparable with the maximum deviation shown in Fig. 9. It allows to speculate that more precise flow front sensors will help to improve the controlled filling even further.

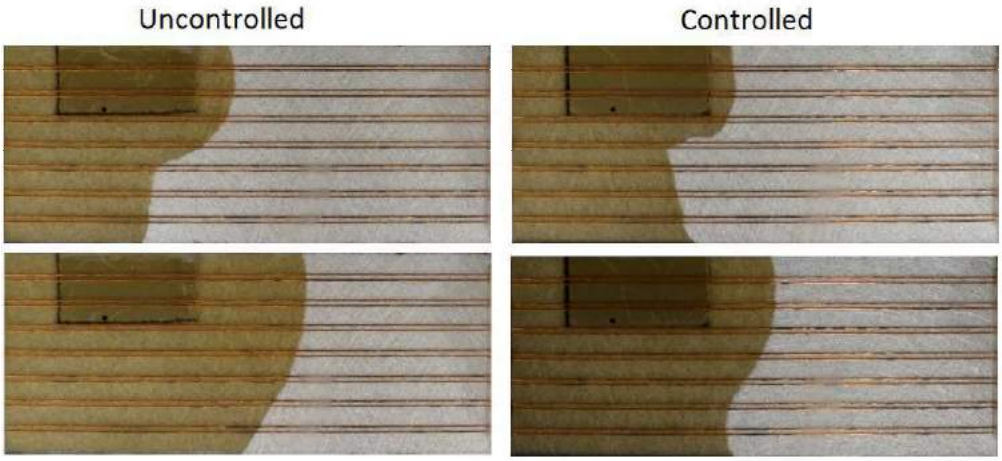

Figure 8: Flow front in uncontrolled and controlled fillings at 18 s (top) and 38 s (bottom) from the start of the experiments.

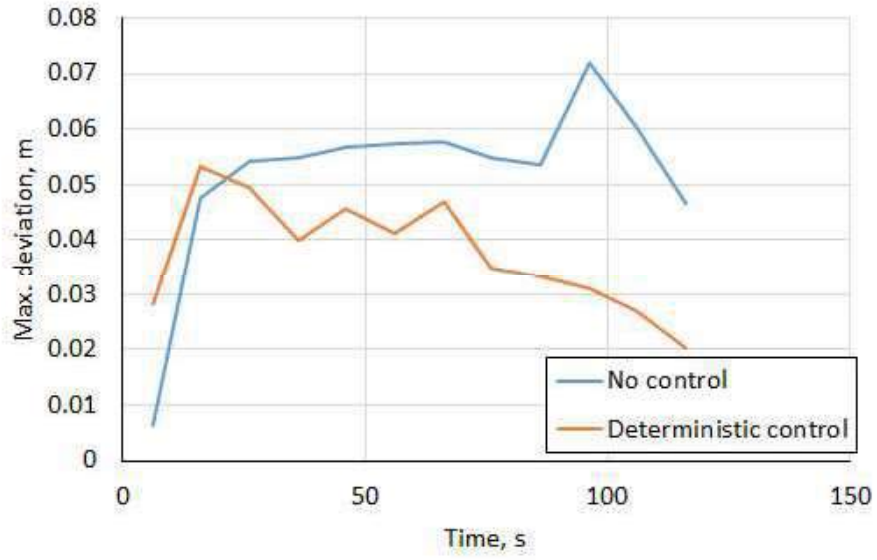

Figure 9: Flow front in uncontrolled and controlled fillings at 18 s (top) and 38 s (bottom) from the start of the experiments.

5. Conclusions

A novel BI algorithm, capable of defect detection in 2D and 3D mould filling problems as shown in [8], was employed for the purpose of control of mould filling processes. It was demonstrated that the proposed implementation of the BI is fast enough for an ACS. The ACS was tested in a virtual environment and showed its ability to control the mould filling time as well as the maximum deviation of the flow front from the desired position.

The experimental validation of the concept showed that an ACS based on physics-based algorithms is feasible in terms of both being sufficiently fast to work with small control step and being able to control the filling time. The experimental validation was performed using only a deterministic algorithm. However, since the stochastic algorithm performed better in the virtual experiment, it is expected that it will also perform better than the deterministic control in a real experiment.

It was noted that excessive errors in the in-process measurement degrade the performance of the ACS since the ACS heavily relies on these input data. This can be mitigated by improving accuracy of flow front sensors and including additional data such as readings from pressure sensors.

Acknowledgment

This work was supported by the Engineering and Physical Sciences Research Council [grant number EP/P006701/1]; through the EPSRC Future Composites Manufacturing Research Hub.

[1] Endruweit, A. and A.C. Long. Infuence of stochastic variations in the fibre spacing on the permeability of bi-directional textile fabrics. Composites Part A. 37 (5): 679-694, 2006.

[2] Mesogitis, T.S., A.A. Skordos, and A.C. Long. Uncertainty in the manufacturing of fibrous thermosetting composites: a review. Composites Part A. 57: 67-75, 2014.

[3] Matveev, M.Y., F. Ball, I.A. Jones, A.C. Long, P.J. Schubel, and M.V. Tretyakov. Uncertainty in geometry of fibre preforms manufactured with Automated Dry Fibre Placement (ADFP) and its effects on permeability. J. Composite Materials. 52(16): 2255-2269, 2018.

[4] Nielsen, D. and R. Pitchumani. Intelligent model-based control of preform permeation in liquid composite molding processes, with online optimization. Composites Part A, 32(12): 1789-1803, 2001

[5] Modi, D., N. Correia, M. Johnson, A. Long, C. Rudd, and F. Robitaille. Active control of the vacuum infusion process. Composites Part A. 38(5): 1271-1287, 2007.

[6] Restrepo, O., K.-T. Hsiao, A. Rodriguez, and B. Minaie. Development of adaptive injection flow rate and pressure control algorithms for resin transfer molding. Composites Part A. 38(6): 1547-1568, 2007.

[7] Iglesias, M.A., M. Park, and M.V. Tretyakov. Bayesian inversion in resin transfer molding. Inverse Problems. 34(10):1005002, 2018.

[8] Matveev M.Y., A. Endruweit, A.C. Long, M.A. Iglesias, and M.V. Tretyakov. Bayesian inversion algorithm for estimating local variations in permeability and porosity of reinforcements using experimental data. In preparation (see Part I of the report).

[9] Luthy, T. and P. Ermanni. Flow monitoring in Liquid Composite Molding based on Linear Direct Current sensing technique. Polymer Composites. 24(2): 249-262, 2003.

[10] Danisman M. Tuncol G., Kaynar A., and Sozer E.M. Monitoring of resin flow in the resin transfer molding (RTM) process using point-voltage sensors. Composites Science and Technology. 67: 367379, 2007.

[11] Advani, S.G. and E.M. Sozer. Process Modeling in Composites Manufacturing. CRC Press, 2010.

[12] Park, M. and M.V. Tretyakov. Stochastic resin transfer molding process, SIAM/ASA J. Uncertainty Quantification. 5: 1110-1135, 2017.

Appendix A. 1D solution

Consider the following 1D problem for resin injection [11, 12]:

$$\begin{aligned} -\frac{d}{dx}K(x)\frac{d}{dx}p(t,x) &= 0,\ 0<x<L(t),\ t>0, \\ p(0,x) &= p_0,\ x\in(0,x_*], \\ p(t,0) &= p_I(t),\ t\geq 0, \\ \frac{d}{dt}L(t) &= -\frac{K(L(t))}{\varkappa(L(t))}\frac{d}{dx}p(t,L),\quad L(0)=0, \\ p(t,L(t)) &= p_0,\ t>0. \end{aligned} \tag{A.1}$$

Here the pressure on the inlet $p_I(t)$ is piecewise-constant left-continuous function on a grid with time step h.

We have

$$K(x)\frac{d}{dx}p(t,x)=C(t)$$

and

$$p(t,x)=p_I(t)+C(t)\int_0^x\frac{dz}{K(z)},$$

which should satisfy the the initial condition and the boundary condition at the front L:

$$p(t,L(t))=p_I(t)+C(t)\int_0^{L(t)}\frac{dz}{K(z)}=p_0.$$

Hence

$$C(t)=\frac{p_0-p_I(t)}{\int_0^{L(t)}\frac{dz}{K(z)}}$$

and thus

$$p(t,x)=p_I(t)-(p_I(t)-p_0)\frac{\int_0^x\frac{dz}{K(z)}}{\int_0^{L(t)}\frac{dz}{K(z)}}.$$

Note that pressure does not depend on porosity explicitly.

We have

$$\begin{aligned} \frac{d}{dt}L(t) &= -\frac{K(L(t))}{\varkappa(L(t))}\frac{d}{dx}p(t,L)=-\frac{K(L(t))}{\varkappa(L(t))}\frac{C(t)}{K(L(t))} \\ &= -\frac{C(t)}{\varkappa(L(t))}=\frac{p_I(t)-p_0}{\varkappa(L(t))\int_0^{L(t)}\frac{dz}{K(z)}} \end{aligned}$$

Hence

$$\int_0^{L(t)}\varkappa(y)\int_0^y\frac{dz}{K(z)}dy=\int_0^t(p_I(s)-p_0)\,ds.$$

Let

$$F(y):=\int_0^y\frac{dz}{K(z)},\ G(x):=\int_0^x\varkappa(y)F(y)dy$$

Then

$$L(t) = G^{-1}\left(\int_0^t (p_I(s) - p_0)\, ds\right)$$

If

$$L(\tau) = x_*, \tag{A.2}$$

$$\int_0^\tau (p_I(s) - p_0)\, ds = G(x_*). \tag{A.3}$$

Suppose we observed at time t_i that the front is at position x_i and we want to find p_I so that the front will be at x_{i+1} at time $t_{i+1} = t_i + h$. We have

$$\int_0^{t_i} (p_I(s) - p_0)\, ds = G(x_i)$$

and

$$\begin{aligned}\int_{t_i}^{t_{i+1}} (p_I(s) - p_0)\, ds &= G(x_{i+1}) - G(x_i) = \int_{x_i}^{x_{i+1}} \varkappa(y)F(y)dy \\ &= (x_{i+1} - x_i)\,\varkappa(x_i)F(x_i) + O\left(x_{i+1} - x_i\right)^2\end{aligned}$$

Since (recall that $p_I(s) = p_I(t_i)$ on $[t_i, t_{i+1}]$)

$$\int_{t_i}^{t_{i+1}} (p_I(s) - p_0)\, ds = (p_I(t_i) - p_0)\, h,$$

$$p_I(t_i) \approx p_0 + \frac{(x_{i+1} - x_i)\,\varkappa(x_i)F(x_i)}{h} \tag{A.4}$$

Note that $K(x)$ here is hydraulic conductivity which is equal to permeability divided by viscosity.

Appendix B. Correction for neighbouring gates

This appendix gives correction of 1D flow which improve the control. To this end, introduce a notion of effective pressure $\tilde{p}_I^i$ at the gate i, which includes a correction to the actual pressure at this gate p_I^i. This notion allows us to decouple estimation of permeability and porosity on different 'lines' corresponding to different gates.

Consider the following correction:

$$\begin{aligned}\tilde{p}_I^i &= \min(p_I^i + \alpha_{ij} \min\left(\frac{(x_j - \Delta_{ij})_+}{\beta_{ij}\Delta_{ij}}, 1\right)(p_I^j - p_I^i)_+ \\ &\quad + \alpha_{ik} \min\left(\frac{(x_k - \Delta_{ik})_+}{\beta_{ik}\Delta_{ik}}, 1\right)(p^k - p_I^i)_+, \max(p_I^i, p_I^j, p_I^k)), \\ i &\neq j,\ j \neq k,\ i \neq k,\ i, j, k = 1, 2, 3,\end{aligned} \tag{B.1}$$

where x_j is a position of the front relative to the gate j, Δ_{ij} are distances between the gates i and j, α_{ij} and β_{ij} are tuning parameters. The parameters β_{ik} (can be replaced by a single parameter β) are related to at what point we think the influence of the other gate is maximal and then not change after that). To start with, we can assume that $\beta_{ik} = \beta = 1$.

The proposed correction has properites consistent with physics of the flow:

- at the start, when $x_j \approx 0$, we have $\tilde{p}_I^i \approx p_I^i$;
- $\tilde{p}_I^i$ are increasing with time as x_j are increasing;

- $\tilde{p}_I^i$ is bounded by $\max(p_I^i, p_I^j, p_I^k)$;
- with time influence of pressure on a gate j on the flow coming from a gate i, $i \neq j$, is increasing until maximum possible pressure is reached.

Let us discuss implementation of (B.1). The use in REnKA is straightforward: just $p_I(t)$ need to be replaced by the corresponding $\tilde{p}_I^i(t)$. The modification to the control part requires further work. First, we substitute $\tilde{p}_I^i(t)$ instead of $p_I(t)$ in the left-hand side of (A.4), i.e., via our control procedure we now find values of the effective pressure $\tilde{p}_I^i(t)$ on the three gates instead of the actual new pressure $p_I^i(t)$ on the gates. Hence, we need to find the three actual new pressure values $p_I^i(t)$ via the computed three effective pressure values $\tilde{p}_I^i(t)$. The easiest is to find $p_I^i(t)$ by using simple iteration. Introduce

$$\begin{aligned}
\Psi_i(p_I^1, p_I^2, p_I^3) \quad : \quad & = \tilde{p}_I^i(t) - \min(\alpha_{ij} \min\left(\frac{(x_j - \Delta_{ij})_+}{\beta_{ij}\Delta_{ij}}, 1\right)(p_I^j - p_I^i)_+ \\
& \quad + \alpha_{ik} \min\left(\frac{(x_k - \Delta_{ik})_+}{\beta_{ik}\Delta_{ik}}, 1\right)(p^k - p_I^i)_+, \max(0, p_I^j - p_I^i, p_I^k - p_I^i)), \\
i \quad \neq \quad & j,\ j \neq k,\ i \neq k,\ i, j, k = 1, 2, 3.
\end{aligned}$$

Set ${}_0p_I^i = p_I^i(t-h)$, i.e. the pressure on the gates from the previous time step and define the interative process:

$$\begin{aligned}
{}_{k+1}p_I^i \quad &= \quad \Psi_i({}_kp_I^1,\ {}_kp_I^2,\ {}_kp_I^3),\ i = 1, 2, 3, \\
k \quad &= \quad 0, 1, \ldots, \overline{k} - 1.
\end{aligned} \tag{B.2}$$

For practical purposes, it is usually sufficient to have $\overline{k} = 2$ or 3. Finally, put

$$p_I^i(t) = {}_{\overline{k}}p_I^i$$

and check that $p_I^i(t) \geq 0$ (if not, close the gate) and that it is not greater than the maximum pressure we can put on the gate (if greater, put the maximum pressure on that gate).